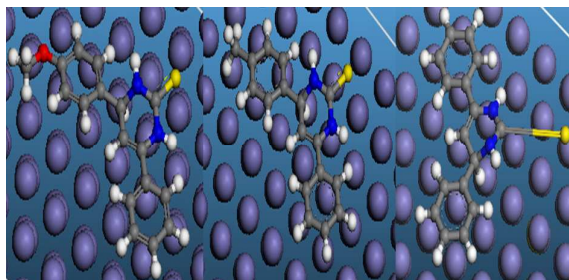




**Pyrimidine-2-thione derivatives as corrosion inhibitors for mild steel in acidic environments**

Journal:	<i>RSC Advances</i>
Manuscript ID:	RA-ART-10-2014-011642.R2
Article Type:	Paper
Date Submitted by the Author:	25-Dec-2014
Complete List of Authors:	Soltani, Nasrin; , Payame Noor University, behpour, mohsen; university of kashan, analytical chemistry Oguzie, Emeka; Federal University of Technology, Owerri, bElectrochemistry and Materials Science Research Laboratory, Department of Chemistry Mahlugi, Meisam; Faculty of Science, University of Kashan, Kashan, I. R. of Iran, Ghasemzade, Ali; Faculty of Science, University of Kashan, Kashan, I. R. of Iran,

## Graphical Abstract



Quantum chemical calculations show that the area containing S atom is possible site for bonding with the mild steel surface.

## Pyrimidine-2-thione derivatives as corrosion inhibitors for mild steel in acidic environments

N. Soltani<sup>a,\*</sup>, M. Behpour<sup>b</sup>, E.E. Oguzie<sup>c</sup>, M. Mahlugi<sup>b</sup>, M.A Ghasemzadeh<sup>b</sup>

<sup>a</sup>Chemistry Department, Payame Noor University, 19395-4697 Tehran, I. R. of Iran

<sup>b</sup>Department of Chemistry, Faculty of Science, University of Kashan, Kashan, I. R. of Iran

<sup>c</sup>Electrochemistry and Materials Science Research Laboratory, Department of Chemistry, Federal University of Technology Owerri, PMB 1526, Owerri, Nigeria

### Abstract

The inhibition of mild steel corrosion in 1.0 M sulphuric acid by pyrimidine-2-thione derivatives (4,6-diphenyl-3,4-dihydropyrimidine-2(1H)-thione (PTH);4-(4-methylphenyl)-6-phenyl-3,4-dihydropyrimidine-2(1H)-thione(PTM) and 4-(4-methoxyphenyl)-6-phenyl-3,4-dihydropyrimidine-2(1H)-thione (PTMO)) has been investigated using weight loss and electrochemical techniques (potentiodynamic polarization and electrochemical impedance spectroscopy (EIS)). All the compounds effectively hindered the corrosion process by becoming adsorbed on the metal surface, following the Langmuir isotherm. Computational studies were undertaken to provide mechanistic insights on the roles of the different substituents on the corrosion inhibition and adsorption behavior of the studied compounds.

*Keywords:* A. Mild steel, B. Polarization, B. EIS, C. Acid inhibition, A. Sulphuric acid.

---

\* Corresponding author:

E-mail: [nasrin\\_soltani2056@yahoo.com](mailto:nasrin_soltani2056@yahoo.com), [nasrin.soltani@pnu.ac.ir](mailto:nasrin.soltani@pnu.ac.ir) (N. Soltani).

Fax number: +98312-5200815

## 1. Introduction

Mild steel is one of the most important iron containing alloys used in different applications. Mild steel is however susceptible to corrosion due to its thermodynamic instability especially in aggressive media <sup>1</sup>. In order to remove unwanted scale and salt deposits or mill scales formed during manufacture, metals are normally immersed in acid pickling baths. Hydrochloric and sulphuric acids are the most commonly used acids in the pickling bath; sulphuric acid being generally preferable because of its lower cost and the non corrosive nature of the  $\text{SO}_4^{2-}$  ion <sup>2,3</sup>. In order to reduce the degree of metal attack and rate of consumption of the acid, corrosion inhibitors are added to the pickling solutions. Most of the well known acid inhibitors are organic compounds containing nitrogen, sulphur and/or oxygen atoms, which facilitate adsorption on the metal surface <sup>4-8</sup>. Furthermore, the nature of adsorption depends on the electronic structure of inhibiting molecules, steric factors, aromaticity and electron density at donor sites, presence of functional groups such as  $-\text{C}=\text{O}$ ,  $-\text{HC}=\text{N}-$ ,  $-\text{N}=\text{N}-$ ,  $\text{R}-\text{OH}$ , etc., molecular area, molecular weight of the molecule, temperature and electrochemical potential at the metal/solution interface <sup>9-14</sup>. It has been reported that S-containing inhibitors are useful in sulphuric acid solution, while N-containing inhibitors exert their best efficiencies in hydrochloric acid <sup>15,16</sup>. On the other hand, compounds containing both nitrogen and sulfur groups generally give rise to satisfactory inhibition efficiency in acidic media <sup>16</sup>.

Recently, some studies have investigated the corrosion inhibition performance of heterocyclic compounds, such as pyrimidine derivatives<sup>3,17-20</sup>, benzimidazole derivatives <sup>21,22</sup>, oxadiazole derivatives <sup>23-25</sup>, oxo-triazole derivatives <sup>26</sup>, pyrazine derivatives <sup>27</sup>, 2-mercaptoimidazole <sup>28</sup>. Despite the relative ease of synthesis of pyrimidine compounds (Scheme 1), as well as their remarkable electronic structures, these compounds have hardly been studied for corrosion inhibition efficacy <sup>2,29</sup>. Accordingly, this study investigates the corrosion of mild steel in  $\text{H}_2\text{SO}_4$  solution in the presence of three pyrimidine-2-thione derivatives (Fig. 1) containing  $-\text{NH}-\text{CS}-\text{NH}$  groups as active centers (compounds containing both nitrogen and sulfur groups). The selected compounds include (4,6-diphenyl-3,4-dihydropyrimidine-2(1H)-thione (PTH);4-(4-methylphenyl)-6-phenyl-3,4-dihydropyrimidine-2(1H)-thione(PTM) and 4-(4-methoxyphenyl)-6-phenyl-3,4-dihydropyrimidine-2(1H)-thione (PTMO)).The choice of this class of compounds is based on molecular structure considerations, i.e., these are organic compounds having the same adsorption centers but they only differ in the substituent at the para position of one of phenyl groups and hence if a difference in the protective properties is observed, it should be predominately attributed to a

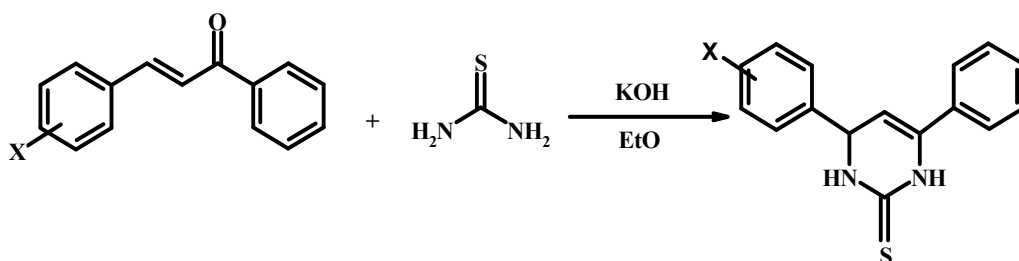
difference in the electronic or steric effect of the substituent type; a structure-activity type relationship. The effect of temperature on corrosion and corrosion inhibition processes was also studied. Computational studies involving quantum chemical calculations and molecular dynamics simulations were employed for establishing the correlation between molecular structure and corrosion inhibiting efficacy.

## 2. Experimental procedures

### 2.1. Materials

#### 2.1.1. Synthesis of Pyrimidine-2-thione derivatives

A mixture comprising of an appropriate chalcone derivative (0.01 mol), thiourea (0.01 mol) and potassium hydroxide (1.0 g) in ethanol (30 ml) was refluxed on a water bath at 70-80 °C for 3 h. Then the reaction mixture was left to stand overnight. The solid separated was dried and crystallized from ethanol. The reaction pathway for preparation of pyrimidine-2-thione derivatives is shown in Scheme 1.



Scheme 1. Schematic representation of preparing process for pyrimidine-2-thione derivatives.

The obtained pyrimidine derivatives were identified by physical and spectroscopic analysis.

#### 2.1.2. Electrodes and Reagents

The employed working electrodes were prepared from a mild steel plate with chemical composition (wt.%): C (0.027), Si (0.0027), P (0.009), Al (0.068), Mn (0.340), S (0.007), Nb (0.003), Cu (0.007), Ni (0.030), Ti (0.003), Cr (0.008), V (0.003) and Fe (balance). Each mild steel coupon was soldered on one surface with an insulated copper wire and carefully coated with epoxy resin, leaving the other surface (which had a surface area of 1 cm<sup>2</sup>) exposed for

corrosion studies. The exposed metal surface was then abraded with different grades of emery papers 150, 320, 400 and 600, respectively and then washed with double distilled water.

Sulphuric acid (H<sub>2</sub>SO<sub>4</sub>) (Merck) was used for the preparation of solutions. 1.0 M sulphuric acid was prepared in double distilled water and was used throughout the studies.

## 2.2. Weight loss measurements

Mild steel coupons with dimensions 1.0 cm × 1.0 cm × 0.02 cm were abraded by a series of emery papers (grades 400–600–800) and then washed with distilled water, degreased with acetone, and finally dried at room temperature. After weighing accurately using a digital balance with sensitivity of ±0.1 mg, the specimens were immersed in a beaker containing 250 ml of 1.0 M H<sub>2</sub>SO<sub>4</sub> without and with different concentrations of the inhibitors using glass hooks and rods. The temperature was controlled at 25 ± 0.1°C using a water thermostat. All the test systems were open to air. After immersion times of 2, 4, 6, 8 and 10 h, the specimens were taken out, washed with bristle brush under running water to remove the corrosion product, dried with a hot air stream, and re-weighed accurately. In order to get good reproducibility, experiments were carried out in triplicate and the average values were obtained. In this present study, the standard deviation values among parallel triplicate experiments were found to be smaller than 5%, indicating good reproducibility. The corrosion rate ( $v$ ) in mg cm<sup>-2</sup> h<sup>-1</sup> is calculated by the following equation<sup>27</sup>:

$$v = \frac{w}{St} \quad (1)$$

where  $w$  is the average weight loss of three parallel mild steel sheets,  $S$  the total area of one mild steel specimen, and  $t$  is immersion time. With the corrosion rate calculated, the inhibition efficiency ( $\eta_w\%$ ) was determined as follows:

$$\eta_w\% = \frac{v_0 - v}{v_0} \times 100 \quad (2)$$

where  $v_0$  and  $v$  are the values of corrosion rate without and with inhibitor, respectively.

Surface coverage ( $\theta$ ) is estimated from  $\eta_w\%/100$  and was evaluated from the weight loss measurements<sup>30</sup>.

Surface coverage ( $\theta$ ) is estimated from  $\eta_w\%/100$  and was evaluated from the weight loss measurements<sup>30</sup>.

$$\theta = \frac{v_0 - v}{v_0} \quad (3)$$

### 2.3. Electrochemical studies

Electrochemical experiments were carried out using an AUTOLAB model PGSTAT 35. The three-electrode cell consists of the mild steel sample as working electrode, a platinum foil as counter electrode, and saturated (3M)Ag/AgCl as reference electrode. All experiments were performed under ambient conditions without stirring. The working electrode was first immersed into the test solution for 30 min to establish a steady state open circuit potential. All electrochemical tests were repeated at least three times.

Potentiodynamic polarization curves were obtained with a scan rate of  $0.5 \text{ mVs}^{-1}$  in the potential range from -250 to +250 mV relative to the corrosion potential. Corrosion current density values were obtained by Tafel extrapolation method. The experiments were run at different temperatures within the range 25-65 °C using a TAMSON model T1000 thermostat.

Impedance measurements were carried out at the open circuit potential ( $E_{ocp}$ ). The alternating current frequency range was extended from 100 kHz to 0.1 Hz, with a 5 mV sine wave as the excitation signals. Impedance data were analyzed using a Pentium IV computer and FRA software.

### 2.4. Quantum chemical calculations

The molecular sketches of molecules were drawn using the GaussView 3.0. All the quantum calculations were performed with complete geometry optimization by means of standard Gaussian98 software package<sup>31</sup>. The study of the relationship between inhibition efficiency of the molecules and their electronic properties was carried out at the level of B3LYP with 6-311G\*\*, and 6-311++G\*\* basis sets and by the semi-empirical method using the Austin Model (AM1) and Parametric Method (PM3) methods. The following quantum chemical indices were taken into consideration: the energy of the highest occupied molecular orbital ( $E_{HOMO}$ ), the energy of the lowest unoccupied molecular orbital ( $E_{LUMO}$ ), energy band gap,  $\Delta E = E_{HOMO} - E_{LUMO}$  and the dipole moment ( $\mu$ ).

Molecular dynamics simulations of the adsorption structures of the different molecules were performed using the density functional theory (DFT) electronic structure program, Forcite, as contained in the Materials Studio 4.0 software (Accelrys, Inc.).

### 2.5. Surface analysis

The surface morphology of the mild steel samples after immersion in 1.0 M sulphuric acid solution with and without inhibitors, was investigated by Ziess Evo 50 XVP instrument. Chemical composition of the same MS surface was recorded by an EDX detector.

### 3. Results and discussion

#### 3.1 Spectroscopic analysis of the pyrimidine derivatives

The physical and spectroscopic data obtained from analysis of the pyrimidine derivatives are as follows: *4,6-diphenyl-3,4-dihydropyrimidine-2(1H)-thione (PTH)*; Yellow crystal; m.p. 182-184 °C (lit.<sup>18</sup> m.p. 184 °C). FT-IR (KBr, cm<sup>-1</sup>): 3173 (NH), 1644 (C=N), 1559, 1478 (C=C), 1183 (C=S). <sup>1</sup>H-NMR (DMSO-d<sub>6</sub>): δ 4.86 (d, 1H, J=5.0 Hz, 4-CH), 5.15 (d, 1H, J=5.0 Hz, 5-CH), 6.78-7.29 (m, 10H, Ar-H), 8.85 (bs, 1H, NH), 9.60 (bs, 1H, NH). <sup>13</sup>C-NMR (DMSO-d<sub>6</sub>): 55.1, 101.6, 126.3, 126.8, 127.2, 128.85, 129.2, 129.3, 133.8, 134.8, 144.5, 175.4.

*4-(4-methylphenyl)-6-phenyl-3,4-dihydropyrimidine-2(1H)-thione (PTM)*; Yellow crystal; mp 197-198 °C. FT-IR (KBr, cm<sup>-1</sup>): 3198 (NH), 1644 (C=N), 1566, 1480 (C=C), 1184 (C=S). <sup>1</sup>H-NMR (DMSO-d<sub>6</sub>): δ 2.03 (s, 3H, CH<sub>3</sub>), 4.86 (d, 1H, J=5.0 Hz, 4-CH), 5.14 (d, 1H, J=5.0 Hz, 5-CH), 6.87-7.29 (m, 9H, Ar-H), 8.85 (bs, 1H, NH), 9.64 (bs, 1H, NH). C-NMR (DMSO-d<sub>6</sub>): 21.2, 56.0, 102.8, 127.4, 127.9, 128.5, 129.5, 130.4, 130.7, 134.9, 138.4, 142.2, 178.1.

*4-(4-methoxyphenyl)-6-phenyl-3,4-dihydropyrimidine-2(1H)-thione (PTMO)*; White crystal; mp 123-125 °C (lit.<sup>19</sup> m.p. 123-124 °C). FT-IR (KBr, cm<sup>-1</sup>): 3149 (NH), 1642 (C=N), 1555, 1479 (C=C), 1182 (C=S). <sup>1</sup>H-NMR (DMSO-d<sub>6</sub>): δ 3.60 (s, 3H -OCH<sub>3</sub>), 5.13 (m, 2H, 4-CH, 5-CH), 6.79-7.25 (m, 9H, Ar-H), 8.62 (bs, 1H, NH), 9.60 (bs, 1H, NH). <sup>13</sup>C-NMR (DMSO-d<sub>6</sub>): 50.2, 56.0, 100.8, 111.6, 121.1, 126.2, 128.8, 129.1, 129.2, 132.1, 134.8, 155.8, 178.2.

#### 3.2. Weight loss measurements

The weight loss of the mild steel test coupons, in g cm<sup>-2</sup> h<sup>-1</sup>, was determined at various time intervals in the absence and presence of different concentrations of inhibitors. The calculated values of corrosion rates ( $v$ ) and surface coverage ( $\theta$ ) obtained from the weight loss measurements at 25 °C are listed in Table 1. It is evident from the results that the corrosion rate decreased with increasing inhibitor concentration and surface coverage ( $\theta$ ) increased with increasing inhibitor concentration, reaching a maximum of 0.99 for the optimum concentration of PTH. The inhibition efficiency of all studied pyrimidine-2-thione derivatives at optimum concentrations (1.00 mM) ranged from 95% to 99%, with the lower limit observed for PTMO. This indicates that the compounds are excellent inhibitors of mild steel corrosion. Moreover, extending the immersion time from 2 h to 10 h did not adversely



affect inhibition performance; rather efficiency even appeared to improve, suggesting stable inhibiting action.

### 3.3. Electrochemical impedance spectroscopy (EIS)

Electrochemical impedance spectroscopy is a veritable tool and has been widely used in investigating corrosion inhibition processes. It provides information on both the resistive and capacitive behaviour at an interface and makes it possible to evaluate the performance of test compounds as possible inhibitors against metal corrosion<sup>32,33</sup>. Fig. 2 (a-c) shows the Nyquist diagrams for mild steel in 1.0 M H<sub>2</sub>SO<sub>4</sub> at 25 °C without and with various concentrations of pyrimidine-2-thione derivatives. The plots maintain similar shapes for all test systems, indicating that the inhibitors do not modify the corrosion mechanism<sup>34</sup>. The impedance spectra generally consist of a large capacitive loop at high frequencies, followed by a small inductive one at low frequencies. The high frequency capacitive loop is related to the charge transfer of the corrosion process and double layer behavior<sup>35</sup>. On the other hand, the low frequency inductive loop may be attributed to relaxation processes associated with adsorption species like FeSO<sub>4</sub><sup>36</sup> or inhibitor species<sup>37</sup> on the electrode surface.

Fig. 3 shows simulated and experimentally generated impedance profiles for mild steel in 1.0 M H<sub>2</sub>SO<sub>4</sub> in the presence of 0.50 mM PTM. It is very clear that the measured impedance response is in accordance with the one calculated by the equivalent circuit shown in Fig. 3a. The circuit consists of the solution resistance  $R_s$ , the charge transfer resistance,  $R_{ct}$ , the constant phase element,  $CPE$  and the inductive elements,  $R_L$  and  $L$ . For the description of a frequency independent phase shift between an applied AC potential and its current response, a constant phase element ( $CPE$ ) is used which is defined in impedance representation as<sup>35</sup>:

$$Z_{CPE} = Y_0^{-1}(j\omega)^{-n} \quad (4)$$

where  $Y_0$  and  $n$  are the  $CPE$  constant and exponent, respectively,  $\omega$  is the angular frequency in  $\text{rad s}^{-1}$  ( $\omega = 2\pi f$ ) and  $j^2 = -1$  an imaginary number. The characteristic frequencies  $f_{\max}$  were obtained from the semicircles maxima and used to calculate the associated capacitance ( $C_{dl}$ ) from the equation<sup>38</sup>:

$$C_{dl} = Y_0(2\pi f_{\max})^{n-1} \quad (5)$$

The values of the electrochemical parameters obtained from Nyquist plots are given in Table 2. Inhibition efficiency ( $\eta_{EIS}\%$ ) was computed from the  $R_{ct}$  values as follows<sup>34</sup>:

$$\eta_{EIS}\% = \frac{R_{ct} - R_{ct}^0}{R_{ct}} \times 100 \quad (6)$$

where  $R_{ct}^0$  and  $R_{ct}$  are the charge transfer resistances in the absence and the presence of inhibitors respectively.

The results in the Table 2 show that  $R_{ct}$  increased with increase in the concentration of pyrimidine-2-thione derivatives which also corresponds with the increase in the diameter of the semicircles, while  $C_{dl}$  decreased with increase in concentration. This behaviour could be related to the formation of an insulated adsorption layer [34], of pyrimidine-2-thione derivatives onto the steel surface leading to the formation of a film which isolates the metal from dissolution and charge transfer. In addition, the more the inhibitor is adsorbed, the greater the thickness of the barrier layer according to the Helmholtz model given in equation (7) [37]:

$$C_{dl} = \frac{\epsilon\epsilon_0 A}{d} \quad (7)$$

where  $d$  is the thickness of the protective layer,  $\epsilon$  is the dielectric constant of the medium,  $\epsilon_0$  is the vacuum permittivity and  $A$  is the effective area of the electrode.

### 3.4. Potentiodynamic polarization measurements

#### 3.4.1. Effect of inhibitor concentration

The potentiodynamic polarization behavior of mild steel was studied in relation to inhibitor type and concentration. Fig. 4 shows the polarization curves of mild steel in 1.0 M  $H_2SO_4$  with different concentrations of pyrimidine-2-thione derivatives. The corresponding polarization parameters, such as corrosion potential  $E_{corr}$ , corrosion current  $I_{corr}$  and Tafel slope ( $b_a$  and  $b_c$ ), are shown in Table 3. The degree of surface coverage ( $\theta$ ) and the percentage of inhibition efficiency ( $\eta_p\%$ ) were calculated using the following equations<sup>39</sup>:

$$\theta = \frac{I_{corr}^0 - I_{corr}}{I_{corr}^0} \quad (8)$$

$$\eta_p\% = \theta \times 100 \quad (9)$$

where  $I_{corr}^0$  and  $I_{corr}$  are corrosion current densities of mild steel in the absence and presence of inhibitor, respectively. The results show that addition of the pyrimidine-2-thione derivatives causes a remarkable decrease in the corrosion rate i.e., shifts the both anodic and cathodic curves to lower current densities. In other words, both cathodic and anodic reactions of the mild steel electrode were drastically limited by the inhibitors. Table 3 shows only slight changes in the anodic and cathodic Tafel slopes for all of inhibited solutions in all concentrations. These results indicate that these inhibitors act by simple blocking the

available surface area and do not alter the metal dissolution mechanism<sup>40</sup>. In other words, these inhibitors decrease the surface area available for corrosion without affecting the mechanism of corrosion and only cause inactivation of a part of the metal surface with respect to the corrosive medium<sup>39</sup>. From Table 3, it is also clear that there is a shift towards cathodic potentials in the values of corrosion potential ( $E_{corr}$ ), which indicates that all studied pyrimidine-2-thione derivatives are mixed type inhibitors, with predominant cathodic effect<sup>41, 42</sup>.

#### 3.4.2. Effect of temperature and kinetic parameters

In order to investigate the effect of temperature on corrosion and corrosion inhibition, polarization experiments were carried out in the absence and presence of inhibitors at temperature range of 25-65 °C. Representative polarization curves are shown in Figs. 5–7, with polarization parameters and inhibition efficiency values presented in Table 4. The trend of inhibition efficiency with rise in temperature reveals some interesting variations for the different compounds; for PTH, the values remained almost unchanged, ranging from 98.7 to 96.2 %. For PTM a slightly more pronounced reduction in efficiency is obvious (98.5 – 83.8%); while a more drastic reduction from 96.6 to 76.8% was obtained for PTMO. Since a decrease in inhibition efficiency with rise in temperature is indicative of physical adsorption, the tendency for chemisorption, or more appropriately, the chemisorption character, reduces in the order PTH > PTM > PTMO. Correspondingly, the tendency to undergo physisorption increases in the same order.

It has been reported that the relation between  $1/T$  and  $\ln I_{corr}$  of the temperature controlled corrosion system is governed by Arrhenius equation (Eq. (10))<sup>43, 44</sup>:

$$\ln I_{corr} = \ln A - \frac{E_a}{RT} \quad (10)$$

where  $I_{corr}$  is the corrosion current density,  $E_a$  is the activation energy of the corrosion reaction and  $A$  is an exponential factor. The relation between  $\ln I_{corr}$  and  $1/T$  of the mild steel corrosion reaction in presence of pyrimidine-2-thione derivatives is represented in Fig. 8, and  $E_a$  values are listed in Table 5. The data of Table 5 shows that the activation energies ( $E_a$ ) of the corrosion of mild steel in 1.0 M  $H_2SO_4$  solution in the presence of the pyrimidine-2-thione derivatives (apart from PTH at low concentrations) are higher than that in the free acid solution indicating that pyrimidine-2-thione derivatives exhibit lowered  $\eta_P$  (%) at elevated temperatures<sup>45, 46</sup>.

### 3.5. Adsorption isotherm considerations

The adsorption behaviour of inhibitor molecules on metal surfaces provides some insight into their inhibition mechanism<sup>47,48</sup>. In order to describe adsorption of the studied pyrimidine-2-thione derivatives on the mild steel surface, several adsorption isotherms were tested and the best fit was obtained with the Langmuir adsorption isotherm given in Eq. (11) as follows<sup>49</sup>:

$$\Gamma = \frac{K_{ads} \Gamma_{max} C}{1 + K_{ads} C} \quad (11)$$

where  $C$  ( $\text{mol dm}^{-3}$ ) is the equilibrium concentration of inhibitor in the bulk solution,  $\Gamma$  ( $\text{mol cm}^{-2}$ ) is its amount adsorbed onto the surface (i.e. its surface concentration),  $\Gamma_{max}$  ( $\text{mol cm}^{-2}$ ) is the maximum value of  $\Gamma$ , and the parameter  $K_{ads}$  ( $\text{dm}^3 \text{mol}^{-1}$ ) reflects the affinity of the inhibitor molecules towards surface adsorption sites. The surface coverage at a particular inhibitor surface concentration could be expressed as  $\theta = \Gamma/\Gamma_{max}$ . Thus, Eq. (11) can be rearranged to give<sup>49,50</sup>:

$$\frac{C}{\theta} = \frac{1}{K_{ads}} + C \quad (12)$$

Values of surface coverage ( $\theta$ ) corresponding to different concentrations of pyrimidine-2-thione derivatives were evaluated from the polarization measurements. The relation between  $C/\theta$  and  $C$  at different temperatures is shown in Fig. 9.

According to Eq. (12),  $K_{ads}$  can be calculated from the intercept on the  $C/\theta$  axis. With the following equation,  $\Delta G_{ads}^0$  can be calculated from  $K_{ads}$ <sup>39</sup>:

$$K_{ads} = \left(\frac{1}{55.5}\right) \exp\left(\frac{-\Delta G_{ads}^0}{RT}\right) \quad (13)$$

where  $R$  is gas constant and  $T$  is absolute temperature of experiment and the constant value of 55.5 is the concentration of water in solution in  $\text{mol dm}^{-3}$ .

The calculated values of  $K_{ads}$  and  $\Delta G_{ads}^0$  are listed in Table 6. Large value of  $K_{ads}$  indicates that the adsorption of three Pyrimidine-2-thione compounds on the metal surface is easily and strongly. According to reports of researchers<sup>51,52</sup> the values of  $\Delta G_{ads}^0$  around  $-40 \text{ kJ mol}^{-1}$  or more negative indicates a chemisorption, which involves electron sharing or transfer from the inhibitor molecule to the metal surface to form a coordinate type of bond; whereas values around  $-20 \text{ kJ mol}^{-1}$  or less negative values belongs to a physical adsorption. Inspection of Table 6 reveals that the  $\Delta G_{ads}^0$  at all temperatures is modestly closer to  $-40 \text{ kJ mol}^{-1}$ .

Therefore, it is concluded that chemical interactions should be dominant for the adsorption of inhibitor molecules on the mild steel surface<sup>53,54</sup>.

### 3.6. Quantum chemical studies and mechanism of corrosion inhibition

In the last few decades, theoretical investigations based on quantum chemical calculations have been proposed as a way for predicting a number of molecular parameters directly related to the corrosion inhibiting property of any chemical compound<sup>55</sup>. Thus, quantum chemical calculations were employed to explain the experimental results obtained in this study and to further propose a suitable mechanism for the inhibition action of pyrimidine-2-thione derivatives on the mild steel surface. The optimized molecular structures of the studied molecules are shown in Fig. 10 and the calculated quantum chemical indices  $E_{HOMO}$ ,  $E_{LUMO}$ ,  $\Delta E$ , dipole moment ( $\mu$ ) are given in Table 7.

The experimental results show that among the three compounds investigated in this study, the inhibition efficiency of PTH and PTM derivatives are approximately the same, whereas that of PTMO derivative, is a little lower. The reactive ability of the inhibitor is considered to be closely related to the frontier molecular orbitals, the HOMO and LUMO. Higher HOMO energy ( $E_{HOMO}$ ) of the molecule means a higher electron donating ability to appropriate acceptor molecules with low-energy empty molecular orbital and thus explains the adsorption on metallic surfaces by way of delocalized pairs of  $\pi$ -electrons. Therefore, an increase in the values of  $E_{HOMO}$  can facilitate adsorption and hence improve the inhibition efficiency<sup>56</sup>.  $E_{LUMO}$ , the energy of the lowest unoccupied molecular orbital signifies the electron accepting tendency of a molecule. The lower the value of  $E_{LUMO}$ , the more probable it is that the molecule would accept electrons<sup>57</sup>. If the organic molecules offer electrons to unoccupied d-orbitals of metals and accept the electrons in the d-orbitals of metals by using antibonding orbitals to form covalent bond, the adsorption process is chemisorption<sup>58</sup>, and there will be an obvious relationship between the inhibition efficiency and quantum chemical indices. However, our experimentally obtained inhibition efficiencies do not correlate well with  $E_{HOMO}$  and  $E_{LUMO}$ , except in the AM1 method. In AM1 method PTH has the highest value of  $E_{HOMO}$  and PTMO has the lowest value of  $E_{HOMO}$ . Low values of the energy gap ( $\Delta E$ ) will provide good inhibition efficiencies, because the excitation energy to remove an electron from the last occupied orbital will be low<sup>59</sup>. The results of Table 7 show that among all of the quantum chemical approaches, only B3LYP/6-311G\*\* and B3LYP/6-311++G\*\* yielded similar values of  $\Delta E$  for PTH and PTM, with that of PTMO being a bit greater. This trend is in good agreement with the experimental results.

Mulliken charge analysis is used to estimate the adsorption centers of inhibitors. Mulliken charges of the atoms are listed in Table 8. The atoms with the highest negative charge are often considered to have the highest tendency to donate electrons to the metal surface<sup>60</sup>. Therefore, the inhibitor is likely to interact with the metal surface through such atoms. By careful comparison of the Mulliken charges for three pyrimidine-2-thione derivatives compounds, it is clear that S atom, N atoms together with some C atoms of benzene rings for three compounds, the methyl carbon (C4) of the PTM and O atom for PTMO have negative charges. These results indicate that these are the atoms with the highest tendency to donate electron pair to the metal surface.

Fukui function is necessary in understanding the local site selectivity. The Fukui function  $f(\vec{r})$  is defined as<sup>61</sup>:

$$f(\vec{r}) = \left( \frac{\partial \rho(\vec{r})}{\partial N} \right)_{V(\vec{r})} \quad (14)$$

The nucleophilic attack Fukui function ( $f(\vec{r})^+$ ) and electrophilic attack Fukui function ( $f(\vec{r})^-$ ) can be calculated as<sup>51</sup>:

$$f_i(\vec{r})^+ = q_i(N+1) - q_i(N) \quad (15)$$

$$f_i(\vec{r})^- = q_i(N) - q_i(N-1) \quad (16)$$

where  $q_i(N+1)$ ,  $q_i(N)$ ,  $q_i(N-1)$  are charge values of atom  $i$  for cation, neutral and anion, respectively. The values of  $f(\vec{r})^+$  and  $f(\vec{r})^-$  are also given in Table 8. The preferred site for nucleophilic attack is the atom or region in the molecule where the value of  $f(\vec{r})^+$  is the highest while the preferred site for electrophilic attack is the atom/region in the molecule where the value of  $f(\vec{r})^-$  is the highest. It is clear from Table 8 that the largest  $f(\vec{r})^+$  and  $f(\vec{r})^-$  values occur on the S atom for three inhibitors. It can be concluded from these results that the S atom is the most active reaction region responsible for both donating and accepting electrons to form coordinate bonds for the adsorption of ABI on iron surface.

Considering the dipole moment ( $\mu$ ) of the molecules, some authors are of the opinion that an increase of the dipole moment leads to decrease of inhibition and vice versa, suggesting that lower values of the dipole moment will favor accumulation of the inhibitor in the surface layer, while other authors believe the reverse to be the case, particularly with respect to dipole-dipole interactions of molecules and metal surface<sup>62,63</sup>.

Such irregularities are often reflected in the literature as regards correlation of dipole moment with inhibition efficiency inhibitor<sup>64</sup> and is as well obvious from Table 7, where the values of  $\mu$  obtained from B3LYP/6-311G\*\* and B3LYP/6-311++G\*\* methods correspond with the

former point of view, while the values of  $\mu$  obtained from AM1 and PM3 agree with the latter opinion.

The effectiveness of an inhibitor can be related with its electronic and spatial molecular structure. In the case of the studied pyrimidine-2-thione derivatives, the atoms and groups that may interact with the electrode surface were obtained from quantum results (geometry of the inhibitor as well as the nature of its frontier molecular orbitals). The frontier molecular orbitals are analyzed in Fig. 11. It could be readily observed that sulfur and nitrogen atoms within the thione moiety have higher charge densities, with the more pronounced contribution from the S atom. The regions of highest electron density are generally the sites to which electrophiles attacked. Therefore the S atom represents the active center, which has the strongest ability of bonding to the metal surface and accounts for the chemisorption tendency of the molecules on the mild steel surface. The results show that LUMO orbitals for all of pyrimidine-2-thione derivatives are localized and saturated around the entire molecule, which would subsequently undergo non specific/non covalent interactions with the metal surface. Non specific interactions between the different molecules and a representative Fe surface were modeled computationally by means of Forcite quench molecular dynamics in the MS Modeling 4.0 software<sup>62, 63, 65</sup>. Details of the computational procedures have been presented elsewhere<sup>66</sup>. The Fe crystal was cleaved along the (110) plane, which is the closest-packed surface of bcc Fe. Calculations were carried out in a 15 x 15 supercell, with vacuum slab of thickness 20 Å, using the Universal force field and the Smart algorithm with NVT ensemble, a time step of 1 fs and simulation time 50 ps. Temperature was fixed at 298 K. The slab position fixed at 1.00 Å. The system was quenched every 500 steps. Energy and temperature fluctuations during molecular dynamics simulations are plotted as functions of simulation time in Figs 12 and 13. Fig. 14 shows the on-top and side views of the optimized Fe-molecule adsorption structures for single molecules of PTH, PTM and PTMO. The molecules can be seen to maintain a flat-lying adsorption orientation on the Fe surface in order to maximize contact, as expected from the delocalization of the electron density around the molecules. The corresponding interaction energies ( $E_{inter}$ ) were computed using the relationship:

$$E_{inter} = E_{total} - (E_{Fe} + E_{molecule}) \quad (17)$$

$E_{total}$ ,  $E_{Fe}$  and  $E_{molecule}$  denote the energies of the adsorbed Fe/molecule couple, the Fe slab and the molecule respectively, which were obtained by averaging the energies of the five structures of the lowest energy. The output from the corresponding univariate analysis is presented in Table 9. Large negative  $E_{inter}$  values are due probably to considerable dispersive interactions induced by the high polarizability of the sulphur and nitrogen atoms in the

molecules; coupled with the delocalization of  $\pi$  electron. All of these contribute to scale up interaction of the molecules with the metal surface, corresponding to an adsorption mechanism involving blocking of active corrosion sites, in agreement with the experimental findings. Strong adsorption of some organic molecules on metal surfaces has been attributed to epitaxial adsorption orientations<sup>66,67</sup>.

The trend of  $E_{inter}$  (PTH < PTM < PTMO) suggests stronger interaction of PTMO with the Fe surface, which is somewhat inconsistent with the experimental findings. This is understandable since the experimentally obtained values of inhibition efficiency are primarily influenced by chemisorptive interactions, whereas the computed  $E_{inter}$  values also took into consideration the non covalent interactions. Moreover, the trend of results suggests that the various substituents in the molecules play an important role in the overall process.

It is generally known that substituents could sterically or electronically modify the interactions between reactants and thereby alter the reaction rates. Both effects actually play significant roles in the interactions of the pyrimidine-2-thione derivatives under study with the mild steel surface, particularly PTMO. Electronically, the electron releasing/activating methoxy group (-OMe) in PTMO would render the molecule more nucleophilic, thereby enhancing its non specific interaction with the metal surface, compared to PTM (with weakly activating -CH<sub>3</sub> substituent) and PTH, with no such substituent. This possibly accounts for the observed trend in  $E_{inter}$  values. On the other hand, S-containing inhibitors are known to be favourably chemisorbed on iron and steel deployed in acidic environments<sup>68,69</sup>. This has been related to formation of Fe-S covalent bonds. Comprehensive computational evidence of such Fe-S covalent interactions can be found in<sup>66, 68</sup> and some references therein. For the pyrimidine-2-thione derivatives, there is thus no doubt that the chemisorption centre is around the S atom of the thione moiety, corresponding to the HOMO locations in Fig. 11. The comparative bulkiness of the methoxy substituent in PTMO will induce some steric hindrance, which would adversely affect the Fe-S covalent bond, hence reducing the strength of the chemisorptive interactions. Since the chemisorptive interaction is the predominant effect influencing the inhibition efficiency of the molecules, the steric effect of the -OMe group would lower the inhibition efficiency of PTMO, in agreement with the experimental findings. Though the electronic and steric effects of the substituents of the pyrimidine-2-thione derivatives are not very pronounced as the inhibition efficiency and  $E_{inter}$  values do not vary so widely, such phenomena are of immense importance from mechanistic point of view.

### 3.7. Surface characterization: SEM-EDX



The scanning electron micrographs (SEM) images were recorded in order to evaluate the conditions of the steel surfaces in contact with  $\text{H}_2\text{SO}_4$  solution. The SEM images of mild steel after immersion in 1.0 M  $\text{H}_2\text{SO}_4$  for 6 h in absence and presence of 1.00 mM of pyrimidine-2-thione derivatives were performed and shown in Fig. 15. It can be seen from Fig. 15 a mild steel samples before immersion seems smooth and appears some abrading scratches on the surface. Figure 15 b shows that the mild steel surface was strongly damaged in  $\text{H}_2\text{SO}_4$  in the absence of inhibitors. Fig. 15c-e shows the steel surface protected after adding 1 mM of inhibitors, it is observed that the surface damage has diminished in comparison to the blank material.

The results of EDX spectra are shown in Fig. 16 a–e. Fig. 16 a is the EDX spectrum of abraded mild steel surface which shows the characteristics peaks of the elements constituting mild steel sample. Fig. 16 b is the EDX spectrum of uninhibited mild steel sample, the peak of sulphur is presence which indicates the breakdown of mild steel surface with sulphuric acid. However, for inhibited solutions (Fig. 16 c–e), the EDX spectra showed an additional peak characteristic for the existence of N (due to the N atoms of the pyrimidine-2-thione derivatives). This data indicates that pyrimidine-2-thione derivatives molecules adsorbed on the mild steel surface with percentage atomic contents listed in Table 10.

#### 4. Conclusions

Three pyrimidine-2-thione derivatives were synthesized and tested as possible corrosion inhibitors for mild steel in 1.0 M  $\text{H}_2\text{SO}_4$  solution. According to results obtained, the following points can be emphasized:

1. Pyrimidine-2-thione derivatives effectively inhibited the corrosion of mild steel in 1.0 M  $\text{H}_2\text{SO}_4$  solutions to different extents, with PTH and PTM being slightly more effective than PTMO.
2. EIS plots indicate that the compounds increased the charge-transfer resistance of the corrosion process via adsorption on the metal/corrosive interface, and hence the inhibition performance improved with inhibitor concentration.
3. Polarization curves demonstrated that the pyrimidine-2-thione derivatives were mixed-type inhibitors for mild steel surface corrosion in the acid solution.
4. The adsorption of pyrimidine-2-thione derivatives was well described by Langmuir isotherm model under all of the studied temperatures.
5. Quantum chemical calculations show that the area containing S atom is most possible site for bonding with the mild steel surface by donating electrons to the metal. Methoxy

substituent-induced steric hindrance was implicated in the reduced inhibition performance of PTMO, although the electron releasing ability of the same methoxy substituent rendered the PTMO molecule more nucleophilic.

### Acknowledgments

Authors would like to appreciate the financial support from Kashan University for provision of laboratory facilities during the period that this research was conducted.

### References

1. M. K. Pavithra, T. V. Venkatesha, K. Vathsala and K. O. Nayana, *Corrosion Science*, 2010, 52, 3811-3819.
2. R. Hasanov, S. Bilge, S. Bilgiç, G. Gece and Z. Kılıç, *Corrosion Science*, 2010, 52, 984-990.
3. N. Caliskan and E. Akbas, *Materials Chemistry and Physics*, 2011, 126, 983-988.
4. N. O. Obi-Egbedi and I. B. Obot, *Corrosion Science*, 2011, 53, 263-275.
5. D. Daoud, T. Douadi, S. Issaadi and S. Chafaa, *Corrosion Science*, 2014, 79, 50-58.
6. B. P. Markhali, R. Naderi and M. Mahdavian, *Journal of Electroanalytical Chemistry*, 2014, 714-715, 56-62.
7. M. A. Hegazy, A. M. Badawi, S. S. Abd El Rehim and W. M. Kamel, *Corrosion Science*, 2013, 69, 110-122.
8. A. Ongun Yüce, B. Doğru Mert, G. Kardaş and B. Yazıcı, *Corrosion Science*, 2014, 83, 310-316.
9. N. Soltani, M. Behpour, S. M. Ghoreishi and H. Naeimi, *Corrosion Science*, 2010, 52, 1351-1361.
10. T. Tüken, F. Demir, N. Kıcır, G. Sığircık and M. Erbil, *Corrosion Science*, 2012, 59, 110-118.
11. K. R. Ansari, M. A. Quraishi and A. Singh, *Corrosion Science*, 2014, 79, 5-15.

12. Y. Tang, F. Zhang, S. Hu, Z. Cao, Z. Wu and W. Jing, *Corrosion Science*, 2013, 74, 271-282.
13. S. Deng, X. Li and X. Xie, *Corrosion Science*, 2014, 80, 276-289.
14. M. A. Hegazy, M. Abdallah, M. K. Awad and M. Rezk, *Corrosion Science*, 2014, 81, 54-64.
15. A. M. Fekry and R. R. Mohamed, *Electrochimica Acta*, 2010, 55, 1933-1939.
16. Y. Tang, X. Yang, W. Yang, Y. Chen and R. Wan, *Corrosion Science*, 2010, 52, 242-249.
17. F. M. Mahgoub, B. A. Abdel-Nabey and Y. A. El-Samadisy, *Materials Chemistry and Physics*, 2010, 120, 104-108.
18. V. S. Reznik, V. D. Akamsin, Y. P. Khodyrev, R. M. Galiakberov, Y. Y. Efremov and L. Tiwari, *Corrosion Science*, 2008, 50, 392-403.
19. K. F. Khaled, *Corrosion Science*, 2011, 53, 3457-3465.
20. M. S. Masoud, M. K. Awad, M. A. Shaker and M. M. T. El-Tahawy, *Corrosion Science*, 2010, 52, 2387-2396.
21. J. Aljourani, M. A. Golozar and K. Raeissi, *Materials Chemistry and Physics*, 2010, 121, 320-325.
22. X. Wang, H. Yang and F. Wang, *Corrosion Science*, 2011, 53, 113-121.
23. F. Bentiss, M. Traisnel, N. Chaibi, B. Mernari, H. Vezin and M. Lagrenée, *Corrosion Science*, 2002, 44, 2271-2289.
24. M. Lebrini, F. Bentiss, H. Vezin and M. Lagrenée, *Applied Surface Science*, 2005, 252, 950-958.
25. F. Bentiss, M. Traisnel and M. Lagrenée, *Corrosion Science*, 2000, 42, 127-146.
26. Z. Tao, S. Zhang, W. Li and B. Hou, *Corrosion Science*, 2009, 51, 2588-2595.
27. S. Deng, X. Li and H. Fu, *Corrosion Science*, 2011, 53, 822-828.

28. R. Álvarez-Bustamante, G. Negrón-Silva, M. Abreu-Quijano, H. Herrera-Hernández, M. Romero-Romo, A. Cuán and M. Palomar-Pardavé, *Electrochimica Acta*, 2009, 54, 5393-5399.
29. N. R. Mohamed, M. M. T. El-Saidi, Y. M. Ali and M. H. Elnagdi, *Bioorganic & Medicinal Chemistry*, 2007, 15, 6227-6235.
30. M. Benabdellah, R. Touzani, A. Dafali, B. Hammouti and S. El Kadiri, *Materials Letters*, 2007, 61, 1197-1204.
31. M. Frisch, G. Trucks, H. Schlegel, G. Scuseria, M. Robb, J. Cheeseman, V. Zakrzewski, J. Montgomery Jr, R. E. Stratmann and J. Burant, *Inc., Pittsburgh, PA*, 1998.
32. D. A. López, S. N. Simison and S. R. de Sánchez, *Electrochimica Acta*, 2003, 48, 845-854.
33. S. A. Umoren, Y. Li and F. H. Wang, *Corrosion Science*, 2010, 52, 2422-2429.
34. S. A. Umoren, Y. Li and F. H. Wang, *Corrosion Science*, 2010, 52, 1777-1786.
35. W. Li, X. Zhao, F. Liu and B. Hou, *Corrosion Science*, 2008, 50, 3261-3266.
36. S. Deng, X. Li and H. Fu, *Corrosion Science*, 2010, 52, 3840-3846.
37. A. K. Singh and M. A. Quraishi, *Corrosion Science*, 2010, 52, 152-160.
38. C. Hsu and F. Mansfeld, *Corrosion*, 2001, 57, 747-748.
39. N. S. Ayati, S. Khandandel, M. Momeni, M. H. Moayed, A. Davoodi and M. Rahimizadeh, *Materials Chemistry and Physics*, 2011, 126, 873-879.
40. C. Cao, *Corrosion Science*, 1996, 38, 2073-2082.
41. O. Riggs Jr, *Houston, TX*, 1973.
42. M. Behpour, S. M. Ghoreishi, N. Mohammadi, N. Soltani and M. Salavati-Niasari, *Corrosion Science*, 2010, 52, 4046-4057.

43. S. M. A. Hosseini, M. Salari, E. Jamalizadeh, S. Khezripour and M. Seifi, *Materials Chemistry and Physics*, 2010, 119, 100-105.
44. M. Behpour, S. M. Ghoreishi, N. Soltani and M. Salavati-Niasari, *Corrosion Science*, 2009, 51, 1073-1082.
45. M. A. Quraishi, A. Singh, V. K. Singh, D. K. Yadav and A. K. Singh, *Materials Chemistry and Physics*, 2010, 122, 114-122.
46. M. G. A. Khedr and A. M. S. Lashien, *Corrosion Science*, 1992, 33, 137-151.
47. L. Narvaez, E. Cano and D. M. Bastidas, *Journal of applied electrochemistry*, 2005, 35, 499-506.
48. N. A. Negm, M. F. Zaki, M. M. Said and S. M. Morsy, *Corrosion Science*, 2011, 53, 4233-4240.
49. S. Ghareba and S. Omanovic, *Corrosion Science*, 2010, 52, 2104-2113.
50. S. Omanovic and S. Roscoe, *Corrosion*, 2000, 56, 684-693.
51. X. Li, S. Deng and X. Xie, *Corrosion Science*, 2014, 81, 162-175.
52. R. Solmaz, *Corrosion Science*, 2014, 81, 75-84.
53. A. Khamis, M. M. Saleh and M. I. Awad, *Corrosion Science*, 2013, 66, 343-349.
54. D. Wang, B. Xiang, Y. Liang, S. Song and C. Liu, *Corrosion Science*, 2014, 85, 77-86.
55. E. Jamalizadeh, A. H. Jafari and S. M. A. Hosseini, *Journal of Molecular Structure: THEOCHEM*, 2008, 870, 23-30.
56. M. Behpour, S. M. Ghoreishi, M. Khayatkashani and N. Soltani, *Materials Chemistry and Physics*, 2012, 131, 621-633.
57. S. John, B. Joseph, K. K. Aravindakshan and A. Joseph, *Materials Chemistry and Physics*, 2010, 122, 374-379.

58. M. Lebrini, F. Robert, H. Vezin and C. Roos, *Corrosion Science*, 2010, 52, 3367-3376.
59. L. Herrag, B. Hammouti, S. Elkadiri, A. Aouniti, C. Jama, H. Vezin and F. Bentiss, *Corrosion Science*, 2010, 52, 3042-3051.
60. I. B. Obot and Z. M. Gasem, *Corrosion Science*, 2014, 83, 359-366.
61. R. G. Parr and W. Yang, *Journal of the American Chemical Society*, 1984, 106, 4049-4050.
62. E. E. Oguzie, C. K. Enenebeaku, C. O. Akalezi, S. C. Okoro, A. A. Ayuk and E. N. Ejike, *Journal of Colloid and Interface Science*, 2010, 349, 283-292.
63. C. Casewit, K. Colwell and A. Rappé, *Journal of the American Chemical Society*, 1992, 114, 10046-10053.
64. S. T. Arab, *Materials Research Bulletin*, 2008, 43, 510-521.
65. C. Casewit, K. Colwell and A. Rappe, *Journal of the American chemical society*, 1992, 114, 10035-10046.
66. E. E. Oguzie, Y. Li, S. G. Wang and F. Wang, *RSC Advances*, 2011, 1, 866-873.
67. H. Heinz, B. L. Farmer, R. B. Pandey, J. M. Slocik, S. S. Patnaik, R. Pachter and R. R. Naik, *Journal of the American Chemical Society*, 2009, 131, 9704-9714.
68. E. Oguzie, S. Wang, Y. Li and F. Wang, *The Journal of Physical Chemistry C*, 2009, 113, 8420-8429.
69. E. E. Oguzie, G. N. Onuoha and A. I. Onuchukwu, *Materials Chemistry and Physics*, 2005, 89, 305-311.

## Figure Captions

Fig. 1. Chemical structures of pyrimidine-2-thione derivatives

Fig. 2. Nyquist plots of mild steel in 1.0 M  $\text{H}_2\text{SO}_4$  with various concentrations of pyrimidine-2-thione derivatives: (a) PTH, (b) PTM, (c) PTMO. ( $\square$ ) 1.0 M  $\text{H}_2\text{SO}_4$  solution, ( $\blacklozenge$ ) 0.01 mM, ( $\blacktriangle$ ) 0.05 mM, ( $\blacksquare$ ) 0.10 mM, ( $\blacksquare$ ) 0.50 mM, ( $\diamond$ ) 1.00 mM.

Fig. 3. Complex plane impedance plot: (a) Nyquist plots; (b) Bode plots, ( $--\circ--$ ) Experimental data and ( $-$ ) Fit data, (c) together with the equivalent circuit used to fit the impedance data, recorded for a mild steel electrode in 1.0 M  $\text{H}_2\text{SO}_4$  solution + 0.50 mM PTM

Fig. 4. Cathodic and anodic polarization curves in 1.0 M  $\text{H}_2\text{SO}_4$  solution with pyrimidine-2-thione derivatives (a) PTH, (b) PTM, (c) PTMO in different concentrations.

( $\text{—}$ ) 1.0 M  $\text{H}_2\text{SO}_4$ , ( $- - -$ ) 0.01 mM, ( $- \cdot - \cdot -$ ) 0.05 mM, ( $\cdot \cdot \cdot \cdot \cdot$ ) 0.10 mM, ( $- \cdot \cdot \cdot -$ ) 0.50 mM, ( $\cdot \cdot \cdot \cdot \cdot$ ) 1.00 mM.

Fig. 5. Effect of temperature on polarization curves of mild steel corrosion rate in free acid solutions and different concentration of PTH.

( $\text{—}$ ) 1.0 M  $\text{H}_2\text{SO}_4$ , ( $- - -$ ) 0.01 mM, ( $- \cdot - \cdot -$ ) 0.05 mM, ( $\cdot \cdot \cdot \cdot \cdot$ ) 0.10 mM, ( $- \cdot \cdot \cdot -$ ) 0.50 mM, ( $\cdot \cdot \cdot \cdot \cdot$ ) 1.00 mM.

Fig. 6. Effect of temperature on polarization curves of mild steel corrosion rate in free acid solutions and different concentration of PTM.

( $\text{—}$ ) 1.0 M  $\text{H}_2\text{SO}_4$ , ( $- - -$ ) 0.01 mM, ( $- \cdot - \cdot -$ ) 0.05 mM, ( $\cdot \cdot \cdot \cdot \cdot$ ) 0.10 mM, ( $- \cdot \cdot \cdot -$ ) 0.50 mM, ( $\cdot \cdot \cdot \cdot \cdot$ ) 1.00 mM.

Fig. 7. Effect of temperature on polarization curves of mild steel corrosion rate in free acid solutions and different concentration of PTMO.

( $\text{—}$ ) 1.0 M  $\text{H}_2\text{SO}_4$ , ( $- - -$ ) 0.01 mM, ( $- \cdot - \cdot -$ ) 0.05 mM, ( $\cdot \cdot \cdot \cdot \cdot$ ) 0.10 mM, ( $- \cdot \cdot \cdot -$ ) 0.50 mM, ( $\cdot \cdot \cdot \cdot \cdot$ ) 1.00 mM.

Fig. 8. Arrhenius plots of  $\ln(I_{corr})$  versus  $1/T$  in the absence and presence of different concentration of inhibitors. ( $\blacklozenge$ ) 1.0 M  $\text{H}_2\text{SO}_4$  solution, ( $\square$ ) 0.01 mM, ( $\blacktriangle$ ) 0.05 mM, ( $\circ$ ) 0.10 mM, ( $\diamond$ ) 0.50 mM, ( $\bullet$ ) 1.00 mM.

Fig. 9. Langmuir isotherms for adsorption of pyrimidine-2-thione derivatives on the mild steel surface: (a) PTH, (b) PTM, (c) PTMO. ( $\blacklozenge$ ) 25°C, ( $\circ$ ) 35°C, ( $\blacktriangle$ ) 45°C, ( $\square$ ) 55°C, ( $\diamond$ ) 65°C.

Fig. 10. Optimized geometry of studied pyrimidine-2-thione derivatives obtained from B3LYP /6-31G\*\* method.

Fig. 11. The HOMO and LUMO orbitals of optimized pyrimidine-2-thione derivatives molecules.

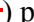



Fig. 12. Energy fluctuations (() potential energy, () kinetic energy, () non-bond energy and () total energy) versus simulation time during molecular dynamics simulations of non-covalent interactions between (a) PTH, (b) PTM, (c) PTMO respectively and the Fe (110) slab

Fig. 13. Temperature fluctuations versus simulation time during molecular dynamics simulations of non-covalent interactions between (a) PTH, (b) PTM, (c) PTMO respectively and the Fe (110) slab

Fig. 14. Optimized adsorption structures for (a) PTH, (b) PTM and (c) PTMO on Fe (110).

Fig. 15. SEM micrographs of the surface of the mild steel specimens after immersion in solutions for 6 h: (a) before corrosion, (b) 1.0 M H<sub>2</sub>SO<sub>4</sub>, (c) 1.0 M H<sub>2</sub>SO<sub>4</sub> containing 1.00 mM PTH, (d) 1.0 M H<sub>2</sub>SO<sub>4</sub> containing 1.00 mM PTM, (e) 1.0 M H<sub>2</sub>SO<sub>4</sub> containing 1.00 mM PTMO.

Fig. 16. EDX spectra of mild steel specimens (a) abraded mild steel (b) uninhibited 1.0 M H<sub>2</sub>SO<sub>4</sub> (c) 1.0 M H<sub>2</sub>SO<sub>4</sub> containing 1.00 mM PTH, (d) 1.0 M H<sub>2</sub>SO<sub>4</sub> containing 1.00 mM PTM, (e) 1.0 M H<sub>2</sub>SO<sub>4</sub> containing 1.00 mM PTMO.



Table 1. Weight loss results of mild steel corrosion in 1.0 M H<sub>2</sub>SO<sub>4</sub> with addition of various concentrations of pyrimidine-2-thione derivatives and in various immersion times.

inhibitor	C (mM)	2h		4h		6h		8h		10 h	
		$v$	$\theta$	$v$	$\theta$	$v$	$\theta$	$v$	$\theta$	$v$	$\theta$
	Blank	3.90	-	8.40	-	10.9	-	15.70	-	19.40	-
PTH	0.01	1.40	0.64	2.82	0.66	3.30	0.70	4.43	0.72	5.36	0.72
	0.05	0.58	0.85	1.19	0.86	1.43	0.87	1.97	0.87	2.06	0.89
	0.10	0.10	0.97	0.15	0.98	0.16	0.99	0.20	0.99	0.42	0.98
	0.50	0.09	0.98	0.18	0.98	0.20	0.98	0.24	0.98	0.33	0.98
	1.00	0.08	0.98	0.14	0.98	0.18	0.98	0.23	0.99	0.19	0.99
PTM	0.01	0.56	0.86	1.16	0.86	1.45	0.87	2.04	0.87	2.30	0.88
	0.05	0.48	0.88	1.00	0.88	1.23	0.89	1.68	0.89	1.95	0.90
	0.10	0.17	0.96	0.30	0.96	0.32	0.97	0.41	0.97	0.33	0.98
	0.50	0.12	0.97	0.20	0.98	0.19	0.98	0.23	0.99	0.12	0.99
	1.00	0.11	0.97	0.13	0.98	0.15	0.99	0.18	0.99	0.16	0.99
PTMO	0.01	1.03	0.74	2.18	0.74	2.74	0.75	3.87	0.75	4.66	0.76
	0.05	0.83	0.79	1.73	0.79	2.16	0.80	3.00	0.81	3.51	0.82
	0.10	0.36	0.91	0.67	0.92	0.77	0.93	1.01	0.94	1.09	0.94
	0.50	0.27	0.93	0.46	0.94	0.50	0.95	0.62	0.96	0.52	0.97
	1.00	0.20	0.95	0.40	0.95	0.47	0.96	0.60	0.96	0.45	0.98

Table 2. Impedance parameters with corresponding inhibition efficiency for the corrosion of mild steel in 1.0 M H<sub>2</sub>SO<sub>4</sub> at different concentrations of pyrimidine-2-thione derivatives.

Inhibitor	<i>C</i> (mM)	<i>R<sub>s</sub></i>	<i>R<sub>ct</sub></i>	<i>Y<sub>0</sub></i> (μF cm <sup>-2</sup> )	<i>n</i>	<i>C<sub>dl</sub></i> (μF cm <sup>-2</sup> )	<i>η<sub>EIS</sub></i> (%)
		( $\Omega$ cm <sup>2</sup> )					
Blank	–	0.17	5.6	695.7	0.86	404.1	-
PTH	0.01	0.22	21.4	345.0	0.87	183.2	73.8
	0.05	0.31	53.8	213.4.1	0.88	96.2	89.6
	0.10	0.42	296.3	108.4	0.89	41.5	98.1
	0.50	0.44	358.4	34.3	0.89	21.3	98.4
	1.00	0.52	449.6	13.1	0.91	8.4	98.7
PTM	0.01	0.34	43.2	239.1	0.86	104.3	87.0
	0.05	0.42	811.9	186.5	0.87	98.8	91.8
	0.10	0.61	138.1	162.3	0.87	61.3	97.3
	0.50	0.84	236.4	120.3	0.88	48.3	98.0
	1.00	0.88	328.9	53.8	0.89	42.4	98.5
PTMO	0.01	0.52	37.8	245.3	0.87	124.5	85.2
	0.05	0.64	49.3	237.7	0.88	98.2	88.6
	0.10	0.83	152.7	196.4	0.88	68.4	96.3
	0.50	0.96	206.4	167.3	0.89	59.2	97.3
	1.00	1.21	298.6	105.8	0.89	41.3	98.1

Table 3. Electrochemical kinetic parameters obtained by Tafel polarization technique for mild steel in absence and presence of various concentrations of pyrimidine-2-thione derivatives in 1.0 M H<sub>2</sub>SO<sub>4</sub> at 25 °C.

Inhibitor	C (mM)	$-E_{corr}$ vs. Ag/AgCl (mV)	$-b_c$	$b_a$	$I_{corr}$ ( $\mu\text{A cm}^{-2}$ )	$\eta_p$ (%)
			————— (mV dec <sup>-1</sup> )			
Blank	–	453	127	95	5970	–
PTH	0.01	439	123	87	1572	73.7
	0.05	434	125	86	631	89.4
	0.10	413	126	92	114	98.0
	0.50	390	135	88	91	98.5
	1.00	387	127	89	76	98.7
PTM	0.01	433	127	96	771	87.1
	0.05	416	125	95	479	92.0
	0.10	406	129	94	173	97.1
	0.50	394	124	93	116	98.1
	1.00	382	123	91	87	98.5
PTMO	0.01	435	124	91	1747	73.7
	0.05	425	129	93	1068	82.1
	0.10	403	127	97	349	94.1
	0.50	399	126	94	273	95.4
	1.00	397	123	90	199	96.6

Table 4 Polarization parameters and corresponding inhibition efficiency for the corrosion of the mild steel in 1.0 M H<sub>2</sub>SO<sub>4</sub> without and with addition of different concentrations of pyrimidine-2-thione derivatives at different temperatures.

inhibitor	C (mM)	Temperature									
		25°C		35°C		45°C		55°C		65°C	
		$I_{corr}$ ( $\mu\text{A cm}^{-2}$ )	$\eta_P$ (%)	$I_{corr}$ ( $\mu\text{A cm}^{-2}$ )	$\eta_P$ (%)	$I_{corr}$ ( $\mu\text{A cm}^{-2}$ )	$\eta_P$ (%)	$I_{corr}$ ( $\mu\text{A cm}^{-2}$ )	$\eta_P$ (%)	$I_{corr}$ ( $\mu\text{A cm}^{-2}$ )	$\eta_P$ (%)
	Blank	5970	-	6210.2	-	14850.2	-	30029.7	-	44870.1	-
PTH	0.01	1572	73.7	1668.4	73.1	2749.6	81.5	5118.4	82.9	5419.9	87.9
	0.05	631	89.4	846.8	86.4	1956.9	86.8	4095.8	86.3	4475.4	90.0
	0.10	114	98.0	503.3	91.9	1288.7	91.3	2573.2	91.4	2324.8	94.8
	0.50	91	98.5	393.7	93.6	1114.4	92.4	1828.9	93.9	1994.2	95.5
	1.00	76	98.7	235.5	96.2	686.3	96.3	1230.6	95.9	1719.7	96.2
PTM	0.01	771	87.1	795.8	87.2	2789.2	81.2	13209.8	56.0	17657.3	60.6
	0.05	479	92.0	715.2	88.5	2259.6	84.9	6521.3	78.3	13478.9	69.9
	0.10	173	97.1	523.3	91.6	2221.8	84.7	2840.9	90.5	10739.7	76.0
	0.50	116	98.1	493.7	92.0	1976.4	86.7	2569.4	91.4	6590.3	85.3
	1.00	87	98.5	385.9	93.7	1273.5	91.4	2113.6	92.9	7249.4	83.8
PTMO	0.01	1747	73.7	1592.4	74.4	3839.8	74.1	6211.3	79.3	28798.2	35.8
	0.05	1068	82.1	1009.8	83.7	2703.4	81.8	3909.9	86.9	21497.6	52.0
	0.10	349	94.1	768.3	87.6	2196.3	85.2	3671.4	87.7	16203.9	63.8
	0.50	273	95.4	622.7	89.9	1858.7	87.5	3209.7	89.3	13498.3	69.9
	1.00	199	96.6	587.2	90.5	1550.5	89.5	2310.5	98.3	11741.8	73.8

Table 5. Activation parameters,  $E_a$  of the dissolution of mild steel in 1.0 M  $H_2SO_4$  in the absence and presence of various concentrations of pyrimidine-2-thione derivatives.

Inhibitor	$C$ (mM)	$E_a$ (kJ mol <sup>-1</sup> )
Blank		46.8
PTH	0.01	30.1
	0.05	46.0
	0.10	65.0
	0.50	65.4
	1.00	66.6
PTM	0.01	75.7
	0.05	74.2
	0.10	83.4
	0.50	82.0
	1.00	88.6
PTMO	0.01	57.5
	0.05	60.8
	0.10	77.1
	0.50	78.8
	1.00	79.6

Table 6. The thermodynamic parameters of adsorption of pyrimidine-2-thione derivatives at different concentrations for mild steel in 1.0 M H<sub>2</sub>SO<sub>4</sub> solution.

inhibitor	Temperature (°C)	$K_{ads} \times 10^5$ (dm <sup>3</sup> mol <sup>-1</sup> )	$R^2$	$-\Delta G_{ads}^0$ (kJ mol <sup>-1</sup> )?
PTH	25	3.03	0.9999	41.2
	35	1.57	0.9998	40.9
	45	1.44	0.9999	42.0
	55	1.84	0.9999	44.0
	65	4.05	0.9978	47.5
PTM	25	4.17	0.9999	42.0
	35	3.30	0.9997	42.6
	45	1.23	0.9998	41.6
	55	1.29	0.9999	43.0
	65	1.25	0.9998	44.3
PTMO	25	1.72	0.9999	39.8
	35	2.56	0.9999	42.2
	45	1.67	0.9998	42.5
	55	0.76	0.9998	41.6
	65	0.39	0.9975	41.0

Table 7. Quantum chemical parameters of used pyrimidine-2-thione derivatives obtained from four quantum methods.

Method	Parameters	Inhibitor		
		PTH	PTM	PTMO
AM <sub>1</sub>	$E_{HOMO}$ (eV)	-0.3275	-0.3281	-0.3353
	$E_{LUMO}$ (eV)	-0.0061	-0.0070	-0.0137
	$\Delta E$ (eV)	0.3214	0.3211	0.3216
	$\mu$ (D)	1.7033	1.6395	1.3071
PM3	$E_{HOMO}$ (eV)	-0.3333	-0.3268	-0.3360
	$E_{LUMO}$ (eV)	-0.0177	-0.0113	-0.0182
	$\Delta E$ (eV)	0.3156	0.3155	0.3178
	$\mu$ (D)	1.5021	1.6524	1.5696
B3LYP/ 6-311G**	$E_{HOMO}$ (eV)	-0.2221	-0.2174	-0.2297
	$E_{LUMO}$ (eV)	-0.0638	-0.0585	-0.0587
	$\Delta E$ (eV)	0.1583	0.1589	0.1710
	$\mu$ (D)	2.7913	5.0890	6.0563
B3LYP/ 6-311++G **	$E_{HOMO}$ (eV)	-0.2262	-0.2228	-0.2333
	$E_{LUMO}$ (eV)	-0.0704	-0.0653	-0.0650
	$\Delta E$ ( eV )	0.1558	0.1574	0.1683
	$\mu$ (D)	2.8189	5.2174	5.7441

Table 8. Quantum chemical parameters of Mulliken charge,  $f_k^+$  and  $f_k^-$  for PTH, PTM ,and PTMO molecules.

PTH					PTM					PTMO							
Atom	$q_N$	$q_{N+1}$	$q_{N-1}$	$f(\vec{r})^+$	$f(\vec{r})^-$	Atom	$q_N$	$q_{N+1}$	$q_{N-1}$	$f(\vec{r})^+$	$f(\vec{r})^-$	Atom	$q_N$	$q_{N+1}$	$q_{N-1}$	$f(\vec{r})^+$	$f(\vec{r})^-$
C (1)	-0.085	-0.063	-0.114	0.022	0.029	C (1)	-0.099	-0.095	-0.103	0.005	0.004	C (1)	-0.088	-0.069	-0.102	0.019	0.014
C (2)	-0.092	-0.075	-0.096	0.0845	-0.824	C (2)	-0.077	-0.051	-0.094	0.026	0.017	C (2)	0.177	0.201	0.155	0.024	0.022
C (3)	-0.088	-0.079	-0.104	0.009	0.016	C (3)	-0.064	-0.053	-0.074	0.011	0.010	C (3)	-0.031	-0.036	-0.027	-0.005	-0.004
C (5)	-0.044	-0.046	-0.042	-0.002	-0.002	C (4)	-0.256	-0.251	-0.259	0.005	0.003	C (5)	-0.131	-0.110	-0.133	0.021	0.002
C (6)	-0.072	-0.059	-0.010	0.013	-0.062	C (5)	-0.037	-0.044	-0.036	-0.007	-0.001	C (6)	-0.089	-0.078	-0.060	0.010	-0.028
C (9)	-0.088	-0.078	-0.045	0.010	-0.043	C (6)	-0.074	-0.056	-0.103	0.019	0.029	O (7)	-0.345	-0.303	-0.361	0.042	0.016
C (12)	0.036	-0.009	-0.023	-0.045	0.059	C (12)	-0.083	-0.070	-0.042	0.013	-0.041	C (9)	-0.076	-0.044	-0.107	0.032	0.031
C (13)	-0.162	-0.084	-0.221	0.078	0.059	C (15)	0.034	-0.013	-0.019	-0.047	0.054	C (10)	0.028	-0.012	0.005	-0.040	0.023
N (14)	-0.393	-0.362	-0.352	0.031	-0.041	C (16)	-0.166	-0.091	-0.225	0.075	0.059	C (11)	-0.133	-0.146	-0.122	-0.012	-0.012
C (16)	0.249	0.124	0.141	-0.125	0.108	N (17)	-0.390	-0.360	-0.353	0.030	-0.036	C (13)	-0.172	-0.111	-0.237	0.061	0.065
C (17)	0.161	0.285	0.241	0.124	-0.080	C (19)	0.249	0.285	0.241	0.036	0.008	N (14)	-0.384	-0.360	-0.365	0.023	-0.019
N (20)	-0.432	-0.379	-0.421	0.053	-0.011	C (20)	0.164	0.123	0.143	-0.041	0.020	C (20)	0.249	0.278	0.242	0.029	0.007
S (22)	-0.273	0.024	-0.460	0.297	0.187	N (23)	-0.432	-0.382	-0.421	0.050	-0.011	C (21)	0.166	0.120	0.150	-0.046	0.015
C (21)	-0.110	-0.097	-0.130	0.013	0.020	C (24)	-0.111	-0.098	-0.130	0.012	0.020	N (24)	-0.433	-0.389	-0.422	0.044	-0.011
C (23)	-0.056	-0.055	-0.094	0.001	0.038	S (25)	-0.276	0.012	-0.462	0.288	0.186	C (25)	-0.111	-0.100	-0.133	0.011	0.022
C (24)	-0.070	-0.043	-0.098	0.027	0.028	C (26)	-0.056	-0.043	-0.098	0.013	0.042	S (26)	-0.278	-0.010	-0.465	0.267	0.187
C (26)	-0.094	-0.078	-0.108	0.016	0.014	C (27)	-0.070	-0.056	-0.094	0.014	0.024	C (27)	-0.070	-0.059	-0.094	0.011	0.024
C (7)	-0.092	-0.080	-0.105	0.012	0.013	C (29)	-0.094	-0.081	-0.105	0.013	0.012	C (28)	-0.056	-0.045	-0.102	0.012	0.045
C (30)	-0.082	-0.052	-0.139	0.030	0.057	C (30)	-0.092	-0.079	-0.109	0.013	0.016	C (30)	-0.092	-0.080	-0.109	0.012	0.017
						C (33)	-0.082	-0.053	-0.139	0.029	0.057	C (31)	-0.094	-0.082	-0.105	0.011	0.011
												C (34)	-0.083	-0.057	-0.141	0.025	0.059



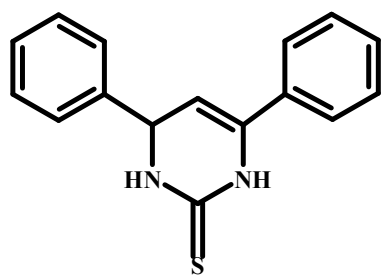
Table 9. Univariate analysis of interaction energies (kcal/mol) from molecular dynamics simulations of non-covalent interactions between PTH, PTM, PTMO respectively and the Fe (110) slab

Parameters	PTH	PTM	PTMO
Number of sample points	5	5	5
Range	3.79700000	1.18300000	4.32900000
Maximum	-42.37000000	-62.19000000	-87.73000000
Minimum	-46.16000000	-63.37000000	-92.05000000
Mean	-44.63000000	-62.99000000	-89.94000000
Median	-44.75000000	-63.22000000	-90.16000000
Variance	1.56000000	0.18830000	2.24800000
Standard deviation	1.39700000	0.48520000	1.67600000
Mean absolute deviation	0.90730000	0.36270000	1.29100000
Skewness	0.58260000	0.74410000	0.07164000
Kurtosis	-1.31600000	-1.38500000	-1.84200000

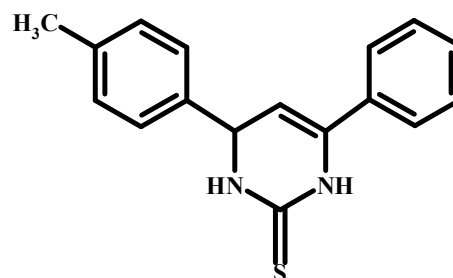
Table 10. Percentage atomic contents of elements obtained from EDX spectra.

Inhibitor	Fe	C	N	O
Abraded mild steel	73.0	21.9	-	4.9
Blank	52.1	40.6	-	7.2
PTH	68.9	26.6	4.4	4.2
PTM	66.5	24.8	4.5	4.1
PTMO	58.9	32.7	4.1	4.1

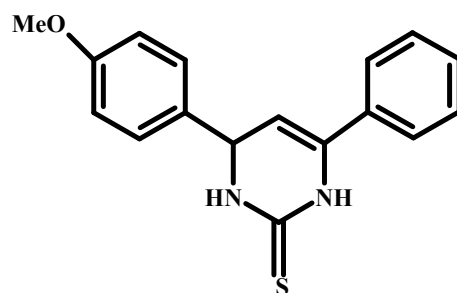
Fig. 1



4,6-diphenyl-3,4-dihydropyrimidine-2  
(1H)-thione  
(PTH)



4-(4-methylphenyl)-6-phenyl-  
3,4-dihydropyrimidine-2(1H)-thione  
(PTM)



4-(4-methoxyphenyl)-6-phenyl-  
3,4-dihydropyrimidine-2(1H)-thione  
(PTMO)

Fig. 2

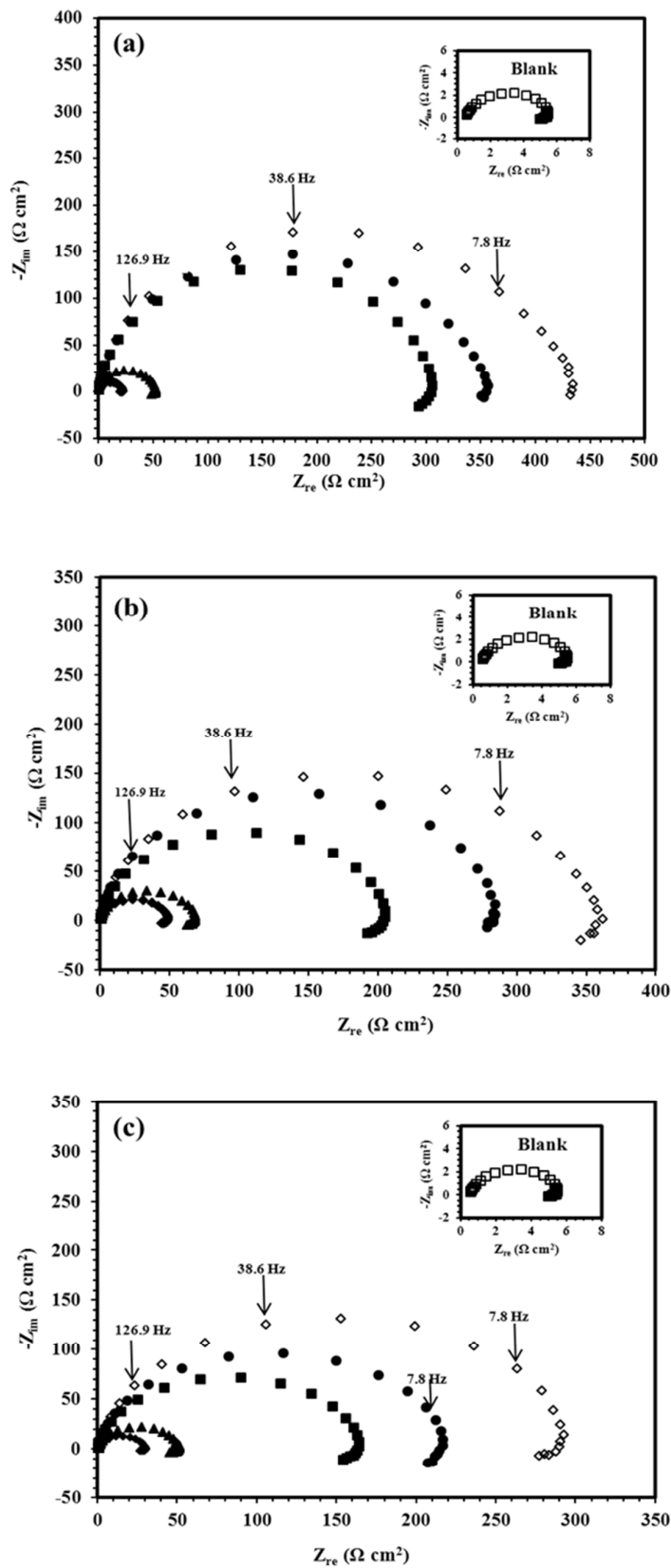


Fig. 3

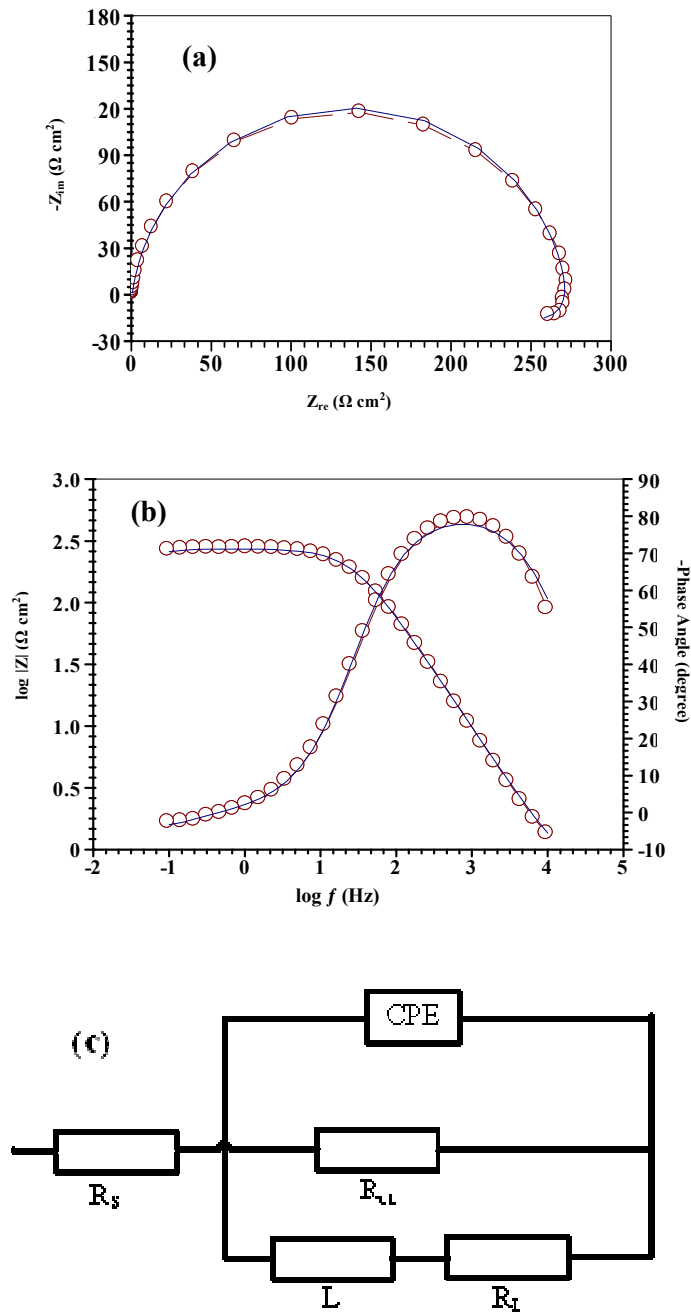


Fig. 4

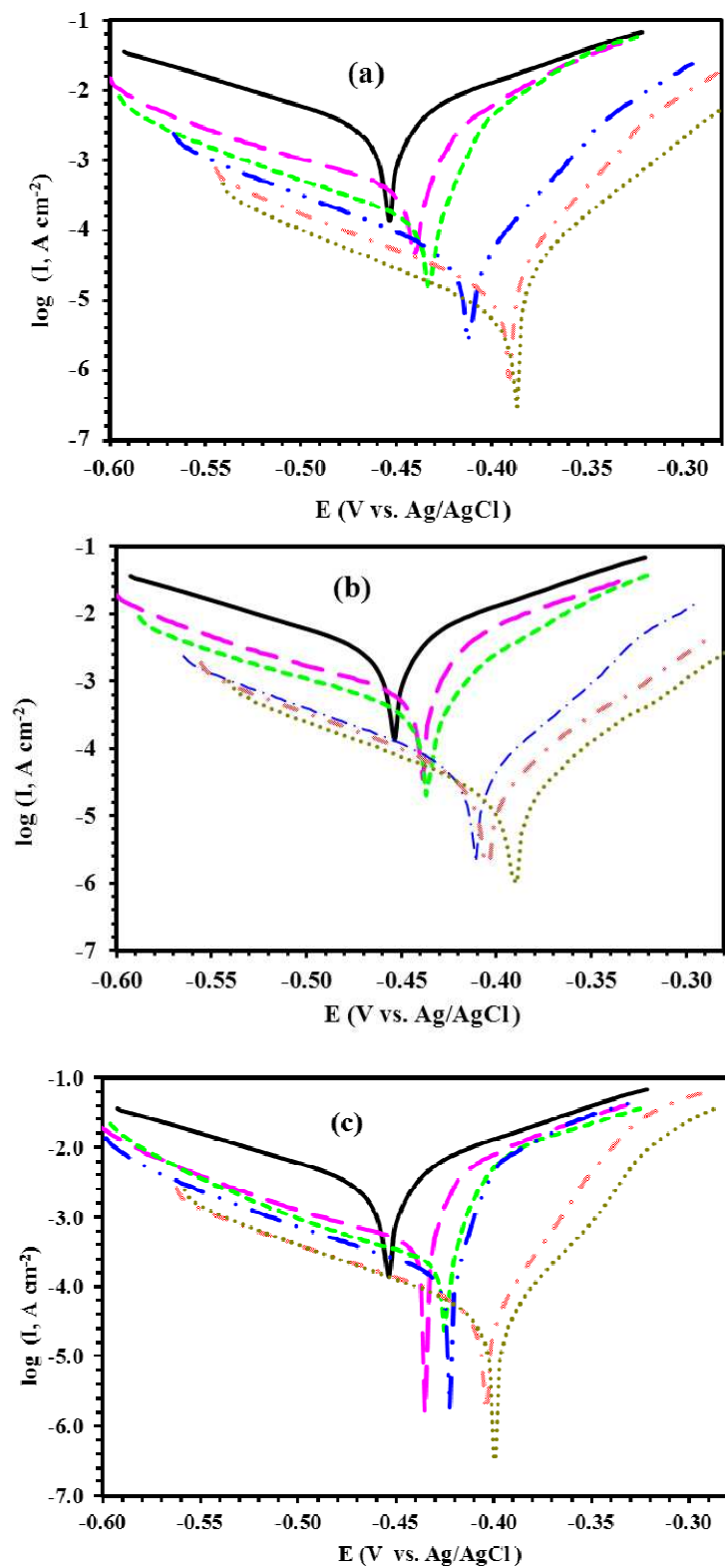


Fig.5

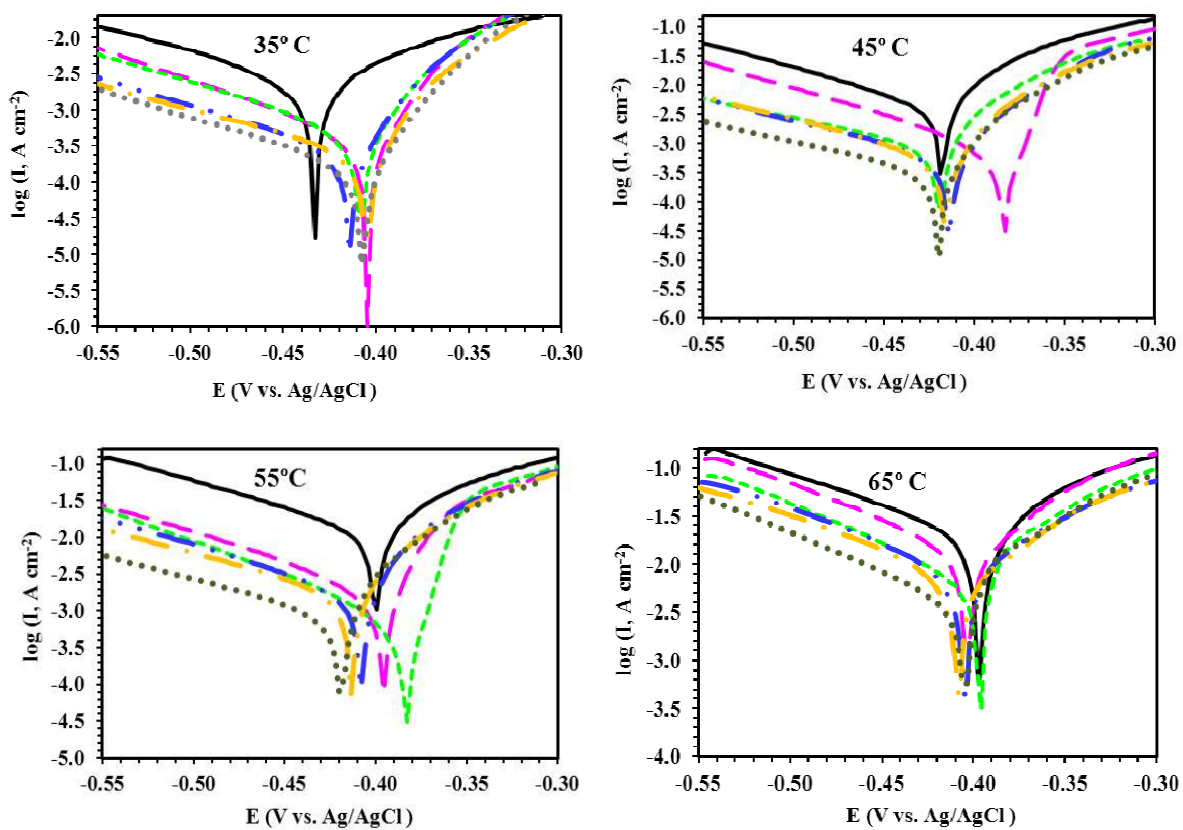


Fig. 6

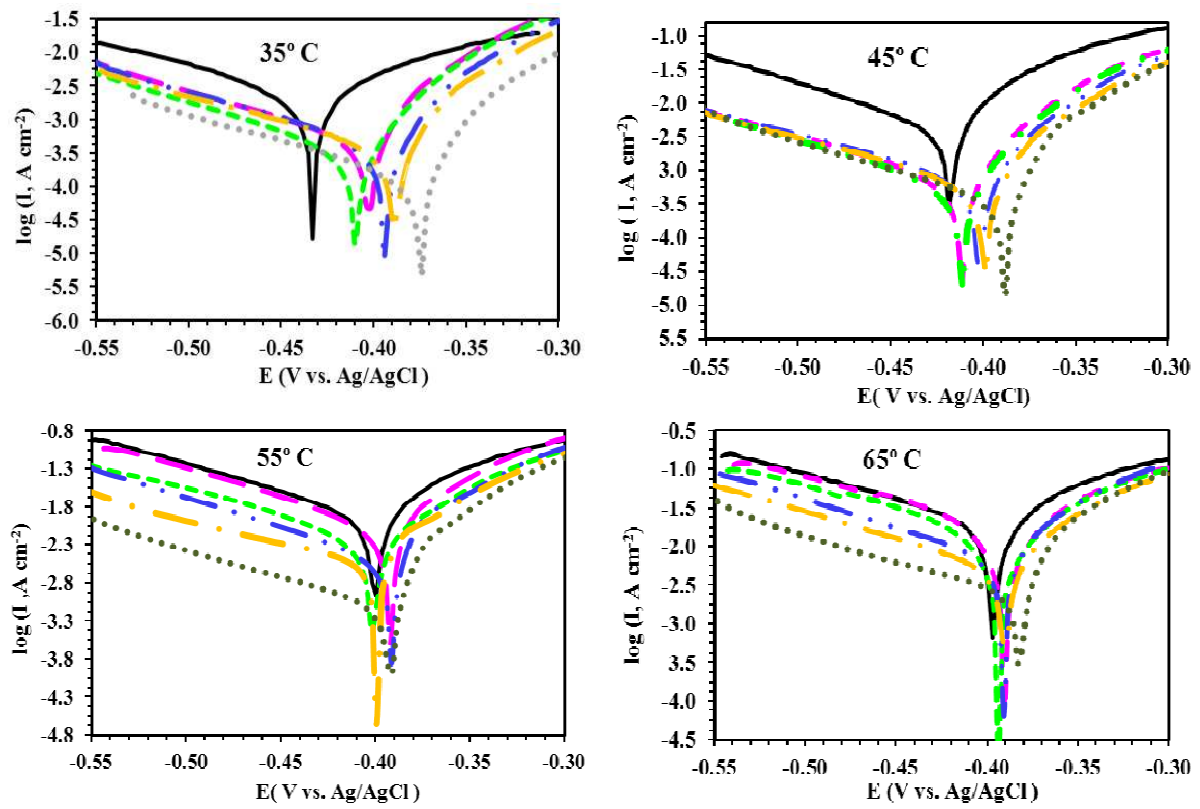




Fig. 7

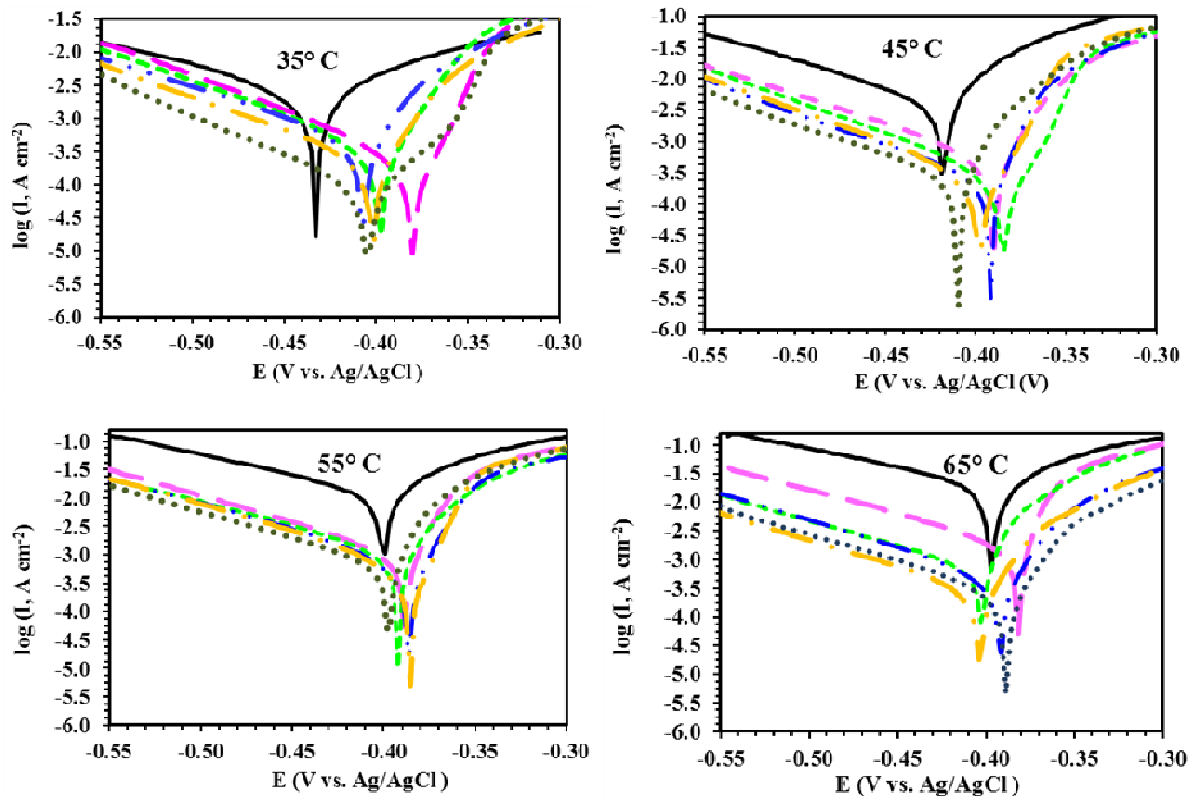


Fig. 8

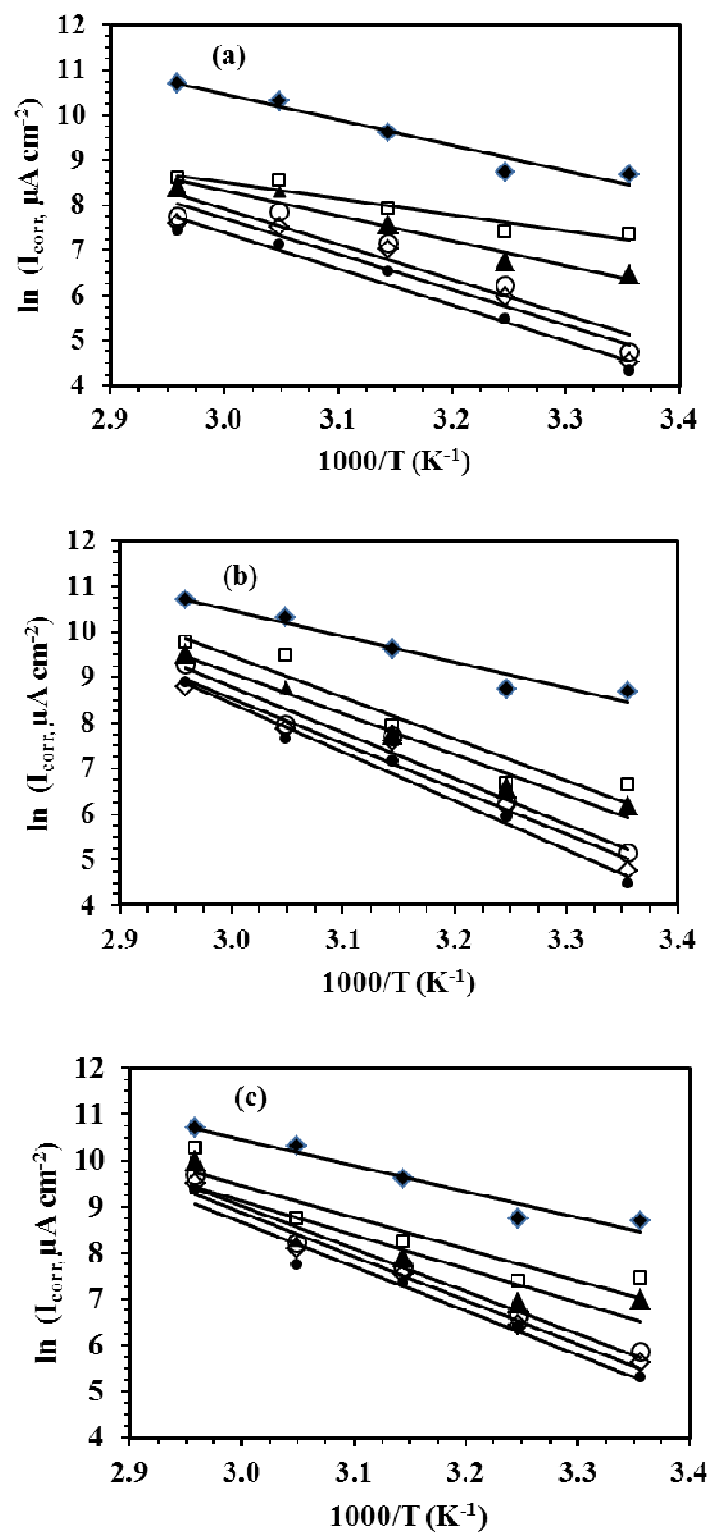


Fig. 9

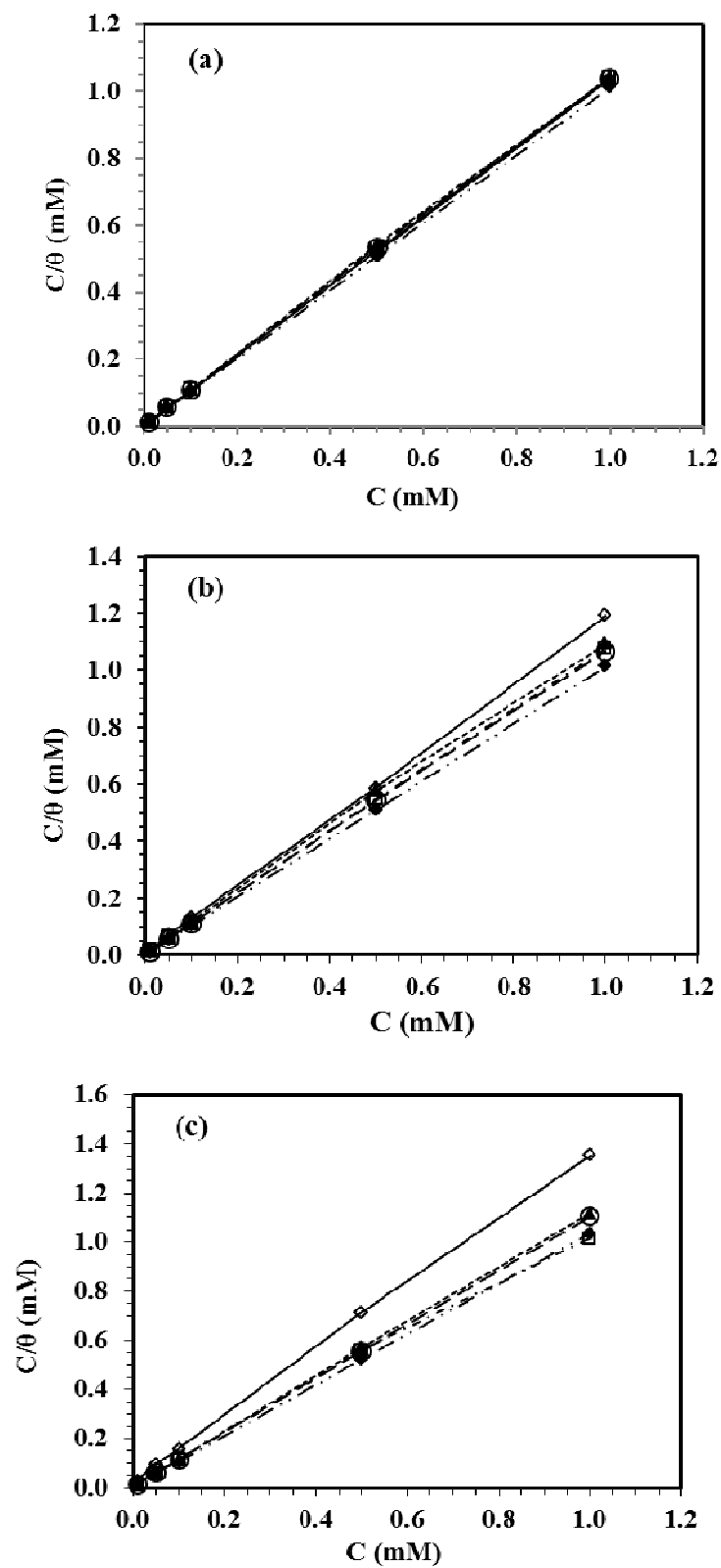


Fig. 10

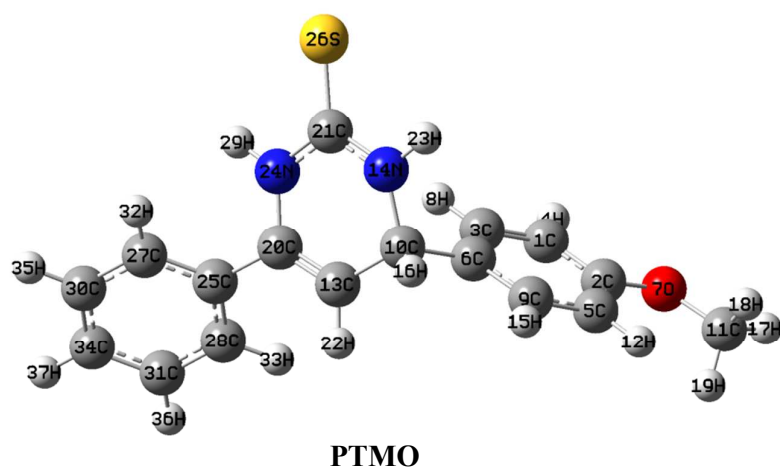
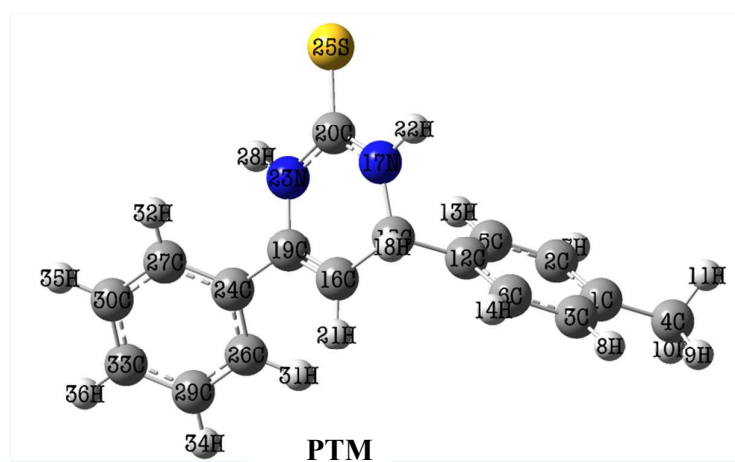
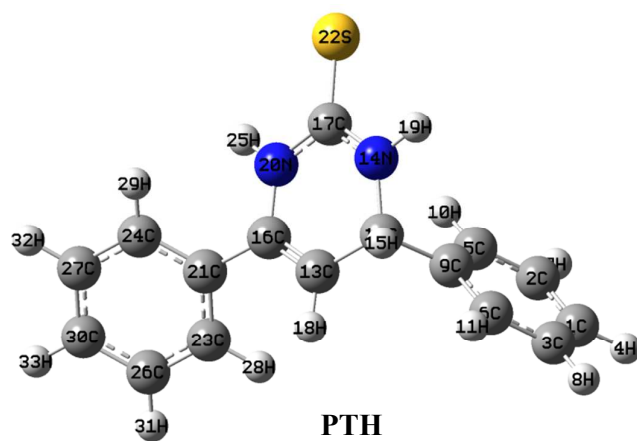


Fig. 11

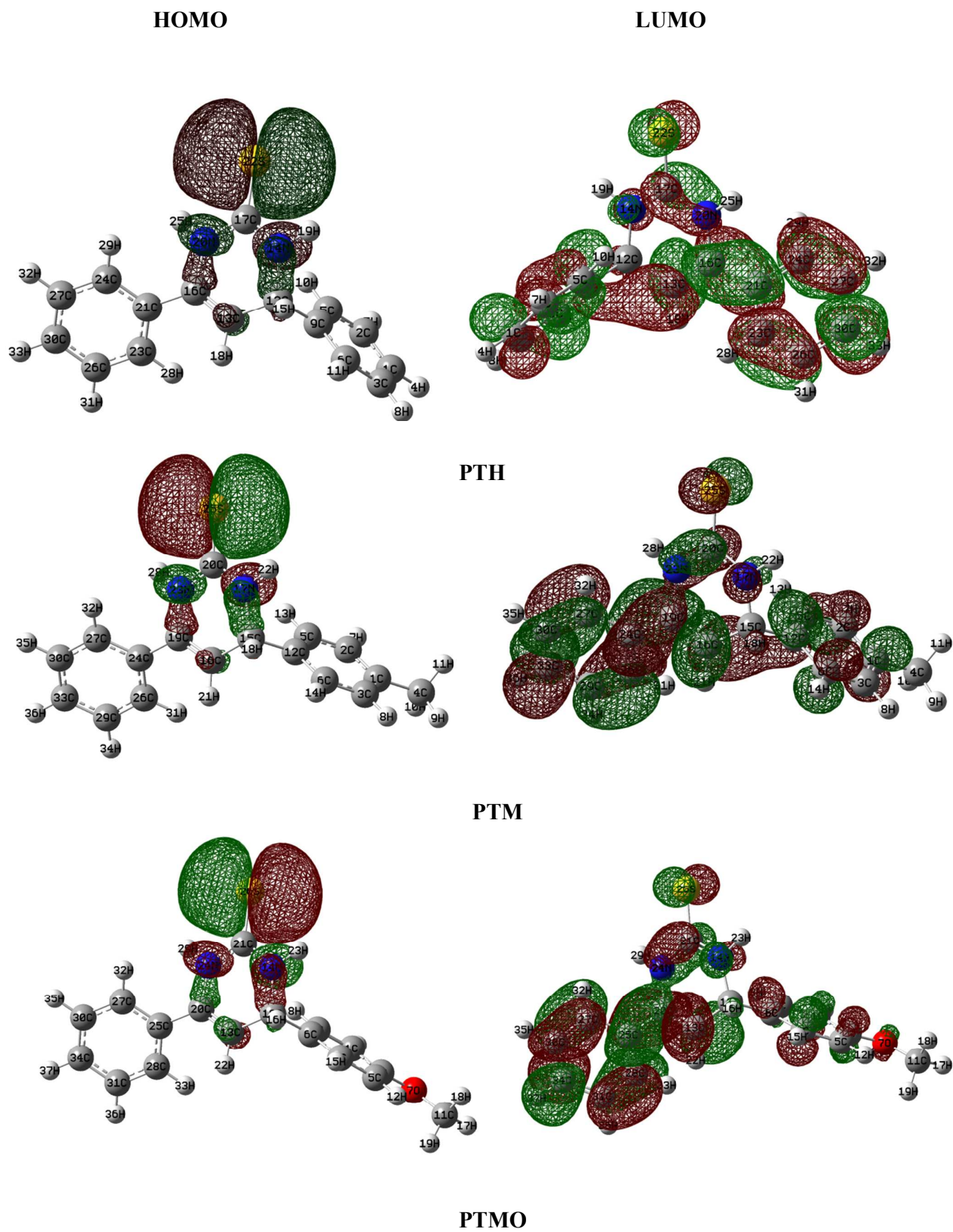


Fig. 12

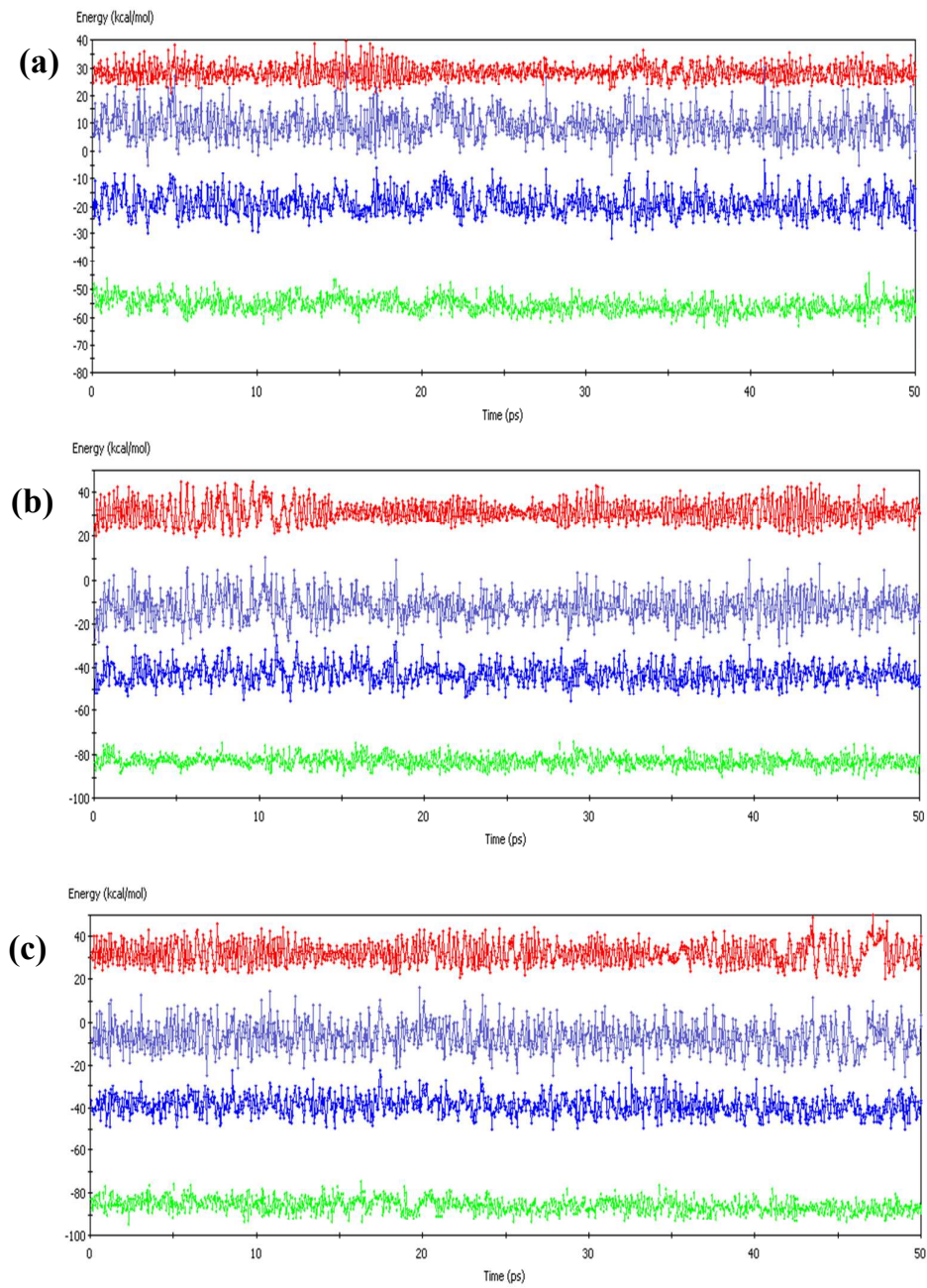


Fig. 13

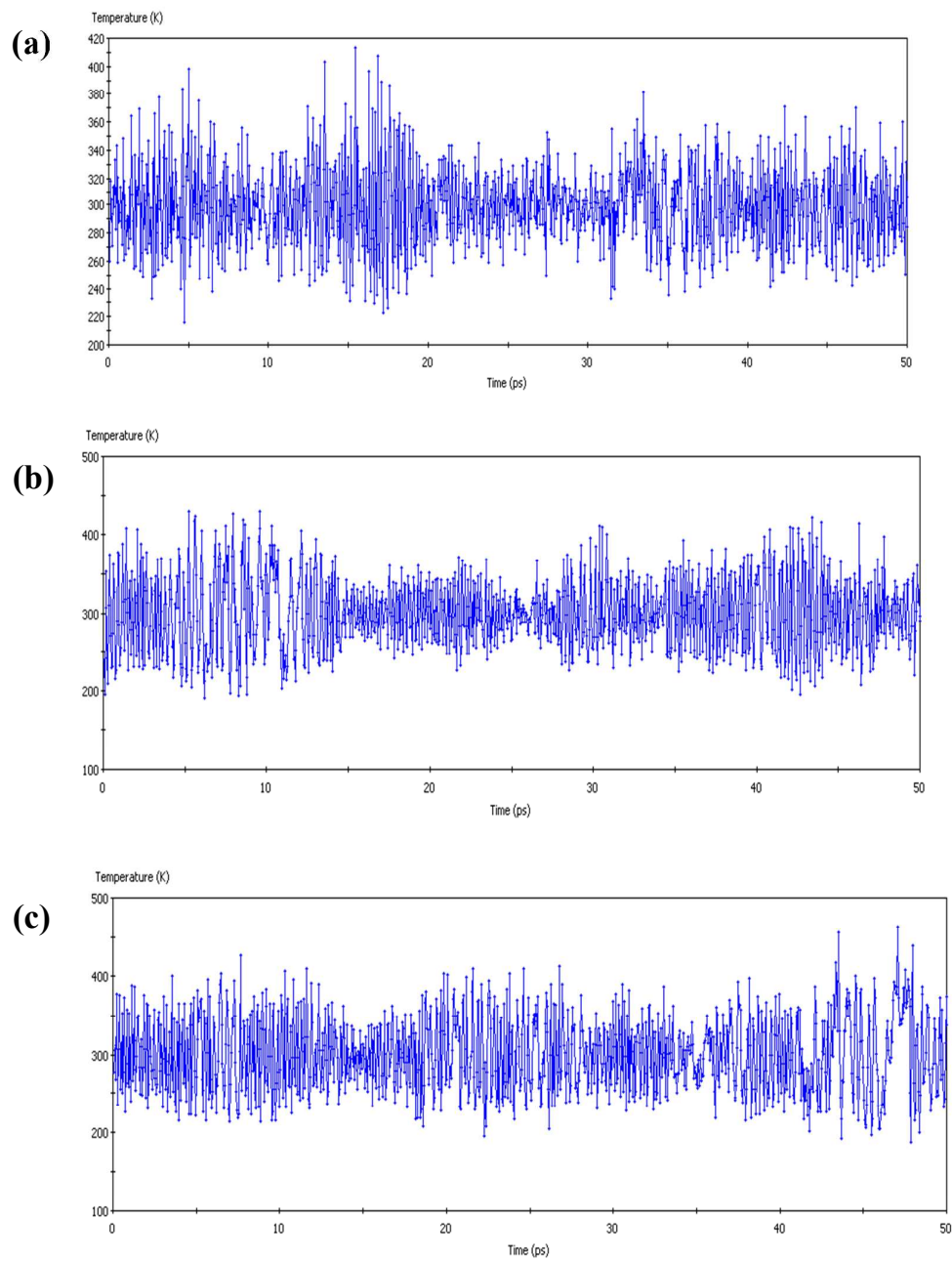


Fig. 14

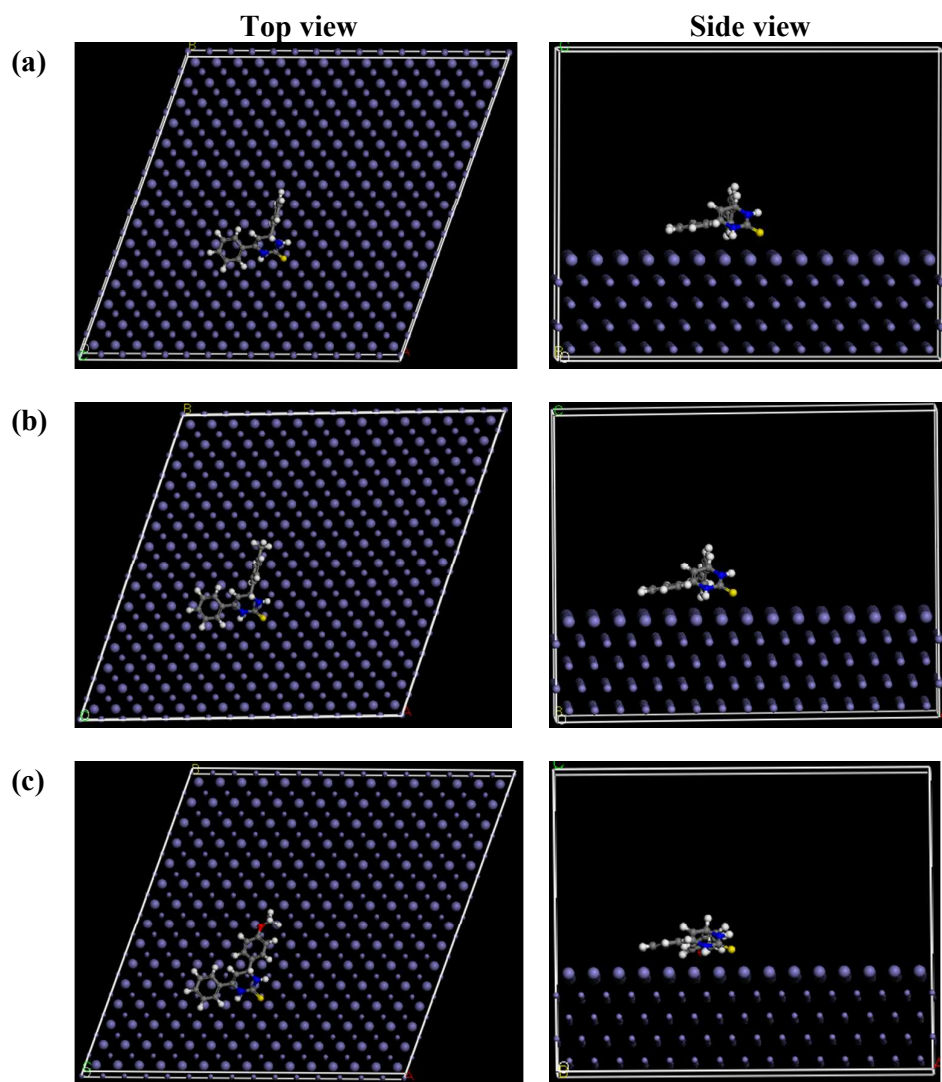




Fig. 15

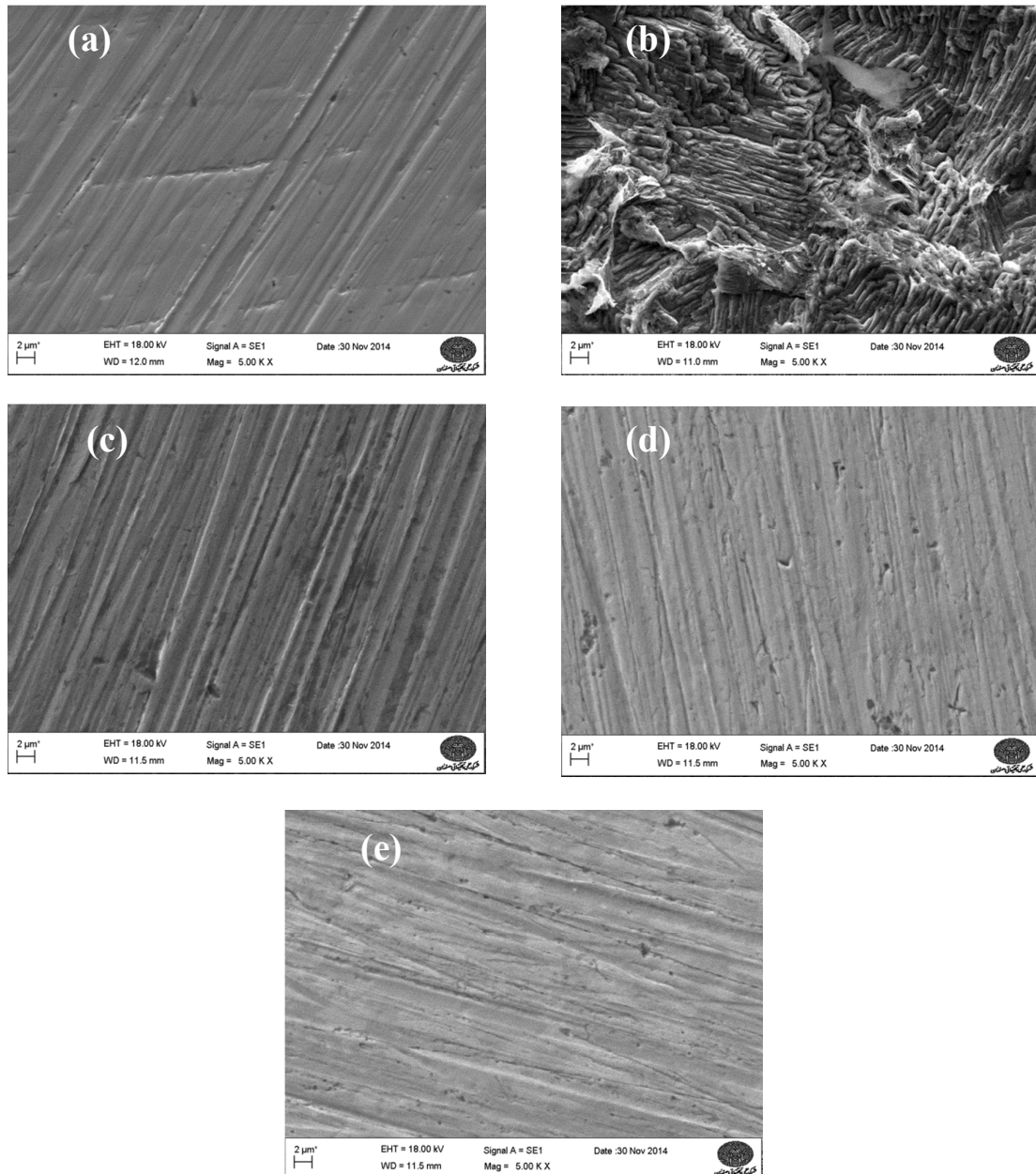


Fig. 16

